Silencing corrugated pipes with liquid addition - Identification of the mechanisms behind whistling mitigation

van Eckeveld, A. C.; Westerweel, J.; Poelma, C.

DOI
10.1016/j.jsv.2020.115495

Publication date
2020

Document Version
Final published version

Published in
Journal of Sound and Vibration

Journal of Sound and Vibration 484 (2020) 115495

Contents lists available at ScienceDirect

Journal of Sound and Vibration

journal homepage: www.elsevier.com/locate/jsvi

Silencing corrugated pipes with liquid addition - Identification of the mechanisms behind whistling mitigation

A.C. van Eckeveld *, J. Westerweel, C. Poelma

Delft University of Technology, Leeghwaterstraat 21, 2628CA, Delft, the Netherlands

ARTICLE INFO

Article history:
Received 11 July 2019
Revised 16 April 2020
Accepted 28 May 2020
Available online 11 June 2020
Handling Editor: O Gottlieb

ABSTRACT

Severe vibrations and sound production can occur in dry gas flow through corrugated pipes. The addition of very small amounts of liquid to the dry gas flow potentially mitigates these *flow-induced vibrations* (FIVs) and noise. The different mechanisms behind this whistling mitigation are studied in this work, where acoustic measurements are combined with flow visualization and droplet sizing. Different corrugation geometries are studied. It is shown that noise mitigation mainly occurs through a geometric alteration of the cavity mouth, resulting in a reduced acoustic source strength. Additional acoustic damping as a consequence of the presence of droplets has a very limited contribution to the mitigation of FIVs. A non-axisymmetric filling of the cavities of a corrugated pipe with liquid is more effective in reducing the acoustic output, compared to an axisymmetric filling. The liquid viscosity has a minor effect on the achieved noise mitigation. To predict the acoustic source strength for a particular cavity geometry a numerical method is developed, based on URANS simulations combined with Howe's energy corollary. An energy balance method is applied to obtain the acoustic source strength from experiments. The whistling frequencies are accurately predicted with the simulations, but the acoustic source strength is over-predicted by a factor 2. Trends in the source strength obtained from simulations, however, closely resemble the experimentally obtained results. The developed method provides an intuitive understanding of sound production by vortical flow structures and shows potential for the prediction of self-sustained oscillations in corrugated pipes.

1. Introduction

Flow-induced vibrations occur in various applications, ranging from wind-turbine noise to building acoustics. One case extensively studied is the aerodynamic noise production from flow over a cavity or a range of cavities. An application that is of particular interest in many fields, and closely related to cavity flow noise, is whistling in corrugated pipes. Corrugated pipes are widely used when a flexible connection is required to transport a gas or liquid from one place to another. The corrugations provide the required flexibility and prevent the pipe from collapsing. The interaction of the internal gas flow with the corrugated pipe wall, which is essentially a sequence of individual axisymmetric cav ities, causes the formation of shear layers over the cavities. These shear layers separate the internal cavity flow from the bulk flow through the pipe. Under certain conditions, they can act as a source of sound. High amplitude acoustic noise is generated, which causes vibrations that can seriously damage

* Corresponding author.
E-mail addresses: andries.van.eckeveld@evides.nl (A.C. van Eckeveld), andriesvaneckeveld@gmail.com (A.C. van Eckeveld).

https://doi.org/10.1016/j.jsv.2020.115495

the system. It is therefore of cardinal importance to understand the whistling phenomenon in corrugated pipe flow and to find ways to mitigate the vibrations that occur.

Noise production in cavity flows is studied widely in literature. A review was provided by Rockwell and Naudascher in the 1970s [1] and more recent contributions are found in the work by Gloerfelt [2]. The sound production observed in cavity flows originates from the unsteady shear layer, separating the low speed inner cavity flow from the higher speed flow over the cavity. Under certain conditions, the shear layer can become unstable, resulting in the formation of discrete vortices [3]. The acoustic amplitude is greatly enhanced if it is strengthened by a feedback mechanism. For low Mach number applications an internal feedback mechanism inside the cavity is generally not dominant. An acoustic feedback can, however, still exist on a larger scale due to the presence of a resonator. When an acoustic resonance is excited by the shear-layer vortices, the acoustics perturbation can synchronize vortex shedding. Examples of these interactions are Helmholtz resonators, where the cavity opening is smaller than the cavity length, and corrugated pipes, where a resonance in the pipe system can occur.

The interaction of vortical structures with the acoustic field in a corrugated pipe is the source of sound [4], which is of dipole nature. Binnie [5] found that the corrugations slightly alter the effective speed of sound (c_{eff}) in the pipe. They provide an additional reactance to the acoustic field, reducing the speed of sound. Elliott [6] derived an expression for this modified speed of sound:

$$c_{\text{eff}} = \frac{c_0}{\sqrt{1 + V_c/(A_p P_c)}}, \tag{1}$$

where V_c is the cavity volume, A_p the inner cross-sectional area of the pipe and P_c the pitch length of the corrugations (see Fig. 3 for a definition sketch). c_0 is the speed of sound at standard conditions. The effective speed of sound, together with the pipe length, determines the resonance frequencies of the entire pipe system, according to:

$$f_r = \frac{n_{\text{ac}} c_{\text{eff}}}{2L_p}, \tag{2}$$

where L_p is the pipe length and $n_{\text{ac}} = 1, 2, 3, \ldots$the mode number. This only holds for axial pipe modes, where the frequency is below the cut-off frequency of the pipe [7]. All transverse pipe modes are evanescent below the cut-off frequency. The present study is limited to frequencies below the cut-off frequency for transverse pipe modes. When whistling occurs, the shedding frequency of the vortices in the cavity mouth locks with one of the acoustic resonance modes of the pipe system.

Maxima of the whistling amplitude in cavity flows are associated with a Strouhal number, which can in first order approximation be estimated by Ref. [8]:

$$Sr_c = \frac{f_w L}{U_b} = 0.13 + 0.40 n_h. \tag{3}$$

In this equation, f_w is the whistling frequency, L a typical cavity length scale, and U_b the bulk velocity through the pipe. $(n_h + 1)$ corresponds to the hydrodynamic mode number, indicating the number of vortices simultaneously present in the cavity mouth. It is shown that the first hydrodynamic mode ($n_h = 0$) is rather weak [9] and that the second hydrodynamic mode is dominant ($n_h = 1$). In practice, instead of the generally unknown vortex convection velocity, the whistling Strouhal number is expressed in terms of the bulk velocity through the pipe: $Sr = \frac{f_w L}{U_b}$. Nakiboğlu et al. [10] found that for corrugations with rounded edges, a modified cavity length ($L = L_c + r_{\text{up}}$, with L_c being the cavity length and r_{up} the upstream cavity edge radius) is the best choice as characteristic length scale. The typical whistling Strouhal number range obtained by Nakiboğlu et al. [10] using this definition is $0.32 \leq Sr \leq 0.42$.

The onset velocity, i.e. the lowest velocity at which stable whistling occurs is related to the relative increase of acoustic losses at lower flow speeds caused the absence of whistling below the onset velocity. The acoustic production is in this case lower than the acoustic losses in the pipe, preventing whistling to occur [11]. After onset, the whistling frequency shows a global characteristic linear increase with flow velocity, corresponding to a fixed Strouhal number. The whistling frequency locks with successive acoustic resonance modes of the pipe, resulting in a step-wise increase of the frequency. Upon increasing the flow velocity the frequency jumps to the next frequency plateau.

In this work we limit ourselves to acoustically compact cavities, excluding cavities in which an internal acoustic feedback mechanism prevails. For these cavities with a depth over length ratio larger than one half ($H_c/L_c > \frac{1}{2}$) the effect of the depth is rather limited [12]. There is a slight influence on the whistling frequency, but the amplitude is largely unaffected. Below this threshold, the whistling amplitude decreases significantly due to the increased interaction between the shear layer and the cavity bottom. The effect of the cavity length relative to the incoming boundary layer thickness is studied widely for flat plate cavities (e.g. by Gharib and Roshko [13]). They showed that the ratio of shear layer length (or cavity length) over incoming boundary layer momentum thickness (L_c/θ) is a crucial parameter, determining whether or not a shear layer becomes unstable and exhibits discrete vortex shedding. For $L_c/\theta > 80$ vortex shedding was observed, in what they called the 'shear layer mode'. Although well established for flat plate cavities, for corrugated pipes this theory has not been verified. However, due to regrowth of the boundary layer over the plateaus separating the corrugations, a similar mechanism is expected in corrugated pipes. The influence of the confinement ratio (i.e. the ratio of pipe diameter to cavity length) is mainly through an alteration of the main stream velocity profile in the pipe [14]. A strong effect of rounding the upstream cavity edge was observed by several authors [5,8,10,15,16]. The whistling amplitude increases when switching from a sharp to a rounded upstream edge. This is due to the

vortex-acoustic field interaction at the upstream edge. The effect of the downstream edge geometry is smaller, because the vortex is less localized once it arrives at this edge.

It is not straightforward to model whistling in corrugated pipes, due to the non-linearity of the phenomenon. Several models are developed to predict the whistling *frequencies* of corrugated systems, for example by Binnie [5], Elliott [6] and Tonon et al. [17]. These models are rather successful. There are also studies focusing on the onset of whistling in corrugated pipes [11] and orifices [18]. The whistling *amplitude*, however, is more difficult to predict. Several semi-emperical models exist (for example the energy balance model by Tonon et al. [17]). These models do require experimental or numerical data on the strength of the acoustic source along the pipe, and obtain the acoustic amplitude by estimating the losses. However, no accurate methods exist that can predict the acoustic amplitude generated by the flow through a corrugated pipe. Experiments or numerical simulations are required to assess the acoustic source power for a specific geometry and flow. Numerical modeling is usually restricted to a decoupled analysis of the flow and the acoustics, using acoustic analogies in combination with Reynolds-averaged Navier-Stokes simulations (RANS), or large eddy simulations (LES) [9,12,19].

Different methods to mitigate whistling in corrugated pipes are proposed in literature. The first study concerning whistling mitigation was carried out by Petrie and Huntley [20]. They found that obstructions in the region of flow separation could strongly reduce the acoustic amplitude. Other authors studied the use of active flow control by means of small speakers in a single corrugation [21], which did not prove to be very effective. Both methods are not applicable in long corrugated pipes. The addition of acoustic damping to the pipe system by means of smooth pipe sections [11] or acoustics dampers is also difficult to implement in many industrial applications. Especially in existing installations, there is a need for an ad-hoc solution which does not require the expensive replacement of entire piping systems.

Liquid addition to the dry gas flow in corrugated pipes provides such a solution. It is shown that the presence of liquid, even at very low liquid fractions, has the potential to mitigate whistling completely [22–24]. The studies by Belfroid et al. [22] and Golliard et al. [23] focused on horizontal pipes, with a limited number of experiments and field cases in vertical pipes. Very small liquid volume fractions ($O(10^{-4})$) were sufficient to remove whistling entirely. The authors proposed several mechanisms causing this whistling mitigation: filling of the cavities with liquid, additional acoustic damping due to the presence of droplets, and a reduction of the acoustic source strength due to shear layer disruption or boundary layer thickening. In a previous work by the authors experiments on a vertically oriented corrugated pipe in upward and downward flow direction are described [24]. It is shown that filling of the corrugations with liquid is an important factor determining the reduction of the whistling amplitude in corrugated pipes. This also explains the observed difference in whistling mitigation between vertical and horizontal pipes: in horizontal pipes a stratified flow regime occurs whereas in vertical pipes the cavities experience predominantly axisymmetric filling. Several open questions still remain. The effect of different corrugation geometries on the sound mitigation by liquid addition is unknown and the contribution of acoustic damping due to the presence of droplets has to be quantified. Furthermore, it is unclear which specific geometrical changes to the cavities cause the whistling mitigation, and what effect changes to the properties (e.g. viscosity and surface tension) of the used liquid have.

This work aims to increase the understanding of whistling mitigation in vertical corrugated pipes by liquid addition. In Section 2 the approach that is followed in this work is explained and a motivation for the different parts is provided. Section 3 discusses the theory required for this work. It introduces the energy balance model and the effect of liquid addition on the acoustics. Subsequently, in Section 4, the experimental setup and measurement techniques are explained. The dry whistling behavior obtained from the experiments for different corrugated pipes is treated in Section 5. This is used as a base case for the experimental results in two-phase conditions (Section 6). The numerical modeling of sound sources in corrugated pipe flow is discussed in Section 7, where the method is explained and numerical results are compared to experiments. Finally, in Section 8 the experimental and the numerical results are discussed, and conclusions and future perspectives are provided in Section 9.

2. Method and motivation

In this work whistling mitigation by liquid addition to vertical corrugated pipe flow is studied. Vertical pipes are studied because in many applications a large part of the pipe is vertical, e.g. in corrugated risers. The purpose of this study is twofold: (1) increasing the understanding of the effect of liquid addition to whistling vertical corrugated pipe flow and (2) developing a numerical tool that potentially predicts the whistling output of corrugated pipes and the effect of liquid addition on that whistling output. This work therefore consists of two parts: an experimental part (Section 4 - 6) and a numerical part (Section 7).

In the experimental study previous work on liquid addition to vertical corrugated pipe flow is extended to several other geometries. Also the effect of liquid properties (mainly viscosity and surface tension) is studied, injecting two different liquids to the corrugated pipe flow. The acoustic output of all geometries is first assessed in single phase conditions (Section 5), providing a reference case for the liquid addition results provided in Section 6. In the experimental study the *energy balance model* (EBM) is applied to deduce an acoustic source power for different corrugation geometries from the acoustic pressure measurements, which will later be compared to the acoustic source power obtained from simulations. Experiments are performed to assess the contribution of different whistling mitigating mechanisms (like droplet damping, cavity filling and the axisymmetry of the cavity filling).

In the numerical part of this work (Section 7) a numerical method is developed and validated, aimed to predict the whistling output of a particular corrugated pipe, and to assess the cavity filling mechanism as important contributor to the whistling mitigation when liquid is added to the corrugated pipe. After validation of the method it is used to provide insight into the

specifics of the whistling cycle in corrugated pipe flow, and the contribution of different parts of the corrugation geometry to the acoustic source power. The scaling of the acoustic source power with the perturbation amplitude and the flow velocity is verified, which is an important assumption in the EBM. The numerical method is subsequently applied to the different corrugation geometries studied experimentally and the numerically obtained acoustic source powers are compared to those obtained from experiments. Finally, the effect of liquid filling of the cavities of a corrugated pipe to the acoustic source power is studied and compared to the experimental results.

Both the experimental and numerical results are discussed in Section 8. A summary of the work is provided in Section 9 and conclusions an future perspectives are given.

3. Theory

The relevant theory is treated in this section. Firstly the *energy balance model* (EBM) is introduced, which is used to estimate the acoustic losses in a corrugated pipe. Subsequently, acoustic damping by a dispersed liquid phase is described, followed by Howe's theory of vortex sound. This theory is used in Section 7 required to obtain the acoustic source strength from simulations.

3.1. Acoustic energy balance

An energy balance model is used to estimate the whistling amplitude in corrugated pipes. This approach, previously described by Tonon et al. [17] and Nakiboğlu et al. [14], is employed to predict the whistling amplitude when the acoustic source strength is known, either from experiments or simulations. The underlying principle is that, when a corrugated pipe exhibits steady whistling, there exists a balance between production and absorption of acoustic energy, determining the whistling amplitude for a specific frequency. The time-averaged acoustic source power along the pipe (originating from the unstable shear layers) is matched by the time-averaged acoustic losses in the entire flow system. The acoustic losses are mainly due to viscothermal losses along the pipe (P_{vt}, due to friction and heat-transfer), radiation losses (P_{rad}) at the entrance and exit of the pipe, and convection losses (P_{conv}) at the outlet of the pipe. Convection losses can also occur at the pipe inlet, depending on the inlet geometry. When this geometry causes flow separation inside the pipe, the acoustic absorption is increased. In the present study acoustic losses due to energy transfer to the pipe wall, resulting in wall-vibrations, is negligible.

Under whistling conditions, the acoustic losses balance the acoustic energy that is generated by the interaction of the flow with the acoustic field in the pipe:

$$\langle P_{\text{source}} \rangle = \langle P_{\text{vt}} \rangle + \langle P_{\text{conv}} \rangle + \langle P_{\text{rad}} \rangle. \tag{4}$$

As the acoustic losses are frequency dependent, the whistling frequency should be known to estimate the source power using this energy balance. This model predicts whether or not a whistling mode can exist for a given frequency and flow rate. Close to the onset of whistling it is rather inaccurate as a consequence of the different amplitude dependency of the source power. The model is applicable in whistling conditions, when the individual terms can be estimated. In the following, each of the terms in Eq. (4) will be derived. First the acoustic sources are treated (the left hand side of the equation), followed by the losses (the right hand side).

3.1.1. Sources

The behavior of the acoustic sources largely depends on the fluctuation amplitude of the acoustic waves that are generated. Three regimes are distinguished, determined by the ratio of the acoustic perturbation amplitude over the flow velocity in the main stream ($|u'|/U_b$) [8]. In the low amplitude regime ($|u'|/U_b < 10^{-3}$), linear theory predicts an exponential amplification of hydrodynamic disturbances of the shear layers, resulting in a growth rate of $e^{2\pi} \approx 500$ over a single hydrodynamic wavelength [25]. The exponential growth imposes a limit to the applicability of the linear theory, since the perturbation amplitude should remain small for the theory to hold. Discrete vortices are formed at higher perturbation levels. The vorticity contained in a hydrodynamic wavelength is then concentrated in these vortices. In the high perturbation amplitude regime (where $|u'|/U_b > 10^{-1}$) the acoustic field directly influences the shear layer behavior, but this regime is not attained in the present work. In the intermediate regime, the strength of the shed vortices does not depend on the perturbation amplitude, because all the vorticity of a hydrodynamic wavelength is concentrated in the coherent vortices. The acoustic source power then scales linearly with $|u'|/U_b$. The boundaries between the different regimes are expected to depend on the geometry and properties of the studied flow.

Following [26], at low Mach numbers, the sound power generated by the vortices is related to the Coriolis force exerted on the acoustic field by the flow:

$$\langle P_{\text{source}} \rangle = -\rho_0 \left\langle \int_V (\boldsymbol{\omega} \times \boldsymbol{u}) \cdot \boldsymbol{u}'_{\text{ac}} dV \right\rangle. \tag{5}$$

Assuming that all vorticity ($\boldsymbol{\omega}$) is concentrated in the vortices means that $\boldsymbol{\omega}$ scales with U_b, as does the flow velocity $\boldsymbol{u}$. The source power then scales as $\langle P_{\text{source}} \rangle = f(\rho_0 U_b^2 u'_{\text{ac}})$. Conversion of the acoustic velocity to a fluctuating pressure (using

$p'_{ac}/(\rho_0 c_{eff}) = u'_{ac}$) and summation over all corrugations yields a description for the acoustic source power of a corrugated pipe:

$$\langle P_{source} \rangle = \frac{2}{\pi} n_c K \rho_0 U_b^3 A_p \frac{c_0}{c_{eff}} \left(\frac{|p'_{max}|}{\rho_0 c_0 U_b} \right), \tag{6}$$

where K is the acoustic source strength constant, which can be obtained from experiments or simulations, and which is geometry specific. n_c is the number of cavities along the pipe, U_b is the bulk gas flow velocity, A_p the cross-sectional area of the pipe, c_0 and c_{eff} are the normal and the effective speed of sound, respectively (see Eq. (1)), ρ_0 the quiescent fluid density, and $|p'_{max}|$ is the maximum amplitude of the acoustic standing pressure wave in the pipe. The factor $2/\pi$ is related to the average amplitude of the sinusoidal standing wave in the pipe: $\overline{|p'_{ac}|} = 2/\pi |p'_{max}|$.

3.1.2. Viscothermal losses

Now that an expression for the acoustic sources is obtained, the acoustic losses are estimated. First the viscothermal losses are treated (the first term on the right hand side of Eq. (4)). These losses occur in the viscous and thermal boundary layers at the pipe wall. The viscothermal losses in the pipe are related to the reduction of the acoustic intensity of sound waves over the pipe length:

$$\langle P_{vt} \rangle = A_p \left[\frac{1}{2} \langle I^+_{in} \rangle - \langle I^+_{out} \rangle \right] + A_p \left[\frac{1}{2} \langle I^-_{in} \rangle - \langle I^-_{out} \rangle \right], \tag{7}$$

where $\langle I^{\pm}_{in} \rangle$ and $\langle I^{\pm}_{out} \rangle$ are the average acoustic intensities for the upstream $(-)$ and downstream $(+)$ traveling waves at the inlet and outlet, respectively. Using the definition of the average intensity $\langle I \rangle$ for plane waves with amplitudes $p'_{\pm}$, being $\langle I^{\pm} \rangle = \frac{|p'_{+}|^2}{2\rho_0 c_0}$, an equation is derived for the viscothermal losses in the main pipe:

$$\langle P_{vt} \rangle = \left[\rho_0 \frac{c_0^2}{c_{eff}} U_b^2 A_p \right] \left(2 - e^{(2\alpha_+ L_p)} - e^{(2\alpha_- L_p)} \right) \left(\frac{|p'_+|}{\rho_0 c_0 U_b} \right)^2, \tag{8}$$

where $\alpha_{\pm}$ are the acoustic damping coefficients for sound waves traveling in the downstream $(+)$ and upstream $(-)$ directions in the pipe, and L_p is the pipe length. It is assumed that the upstream and downstream traveling waves are of equal amplitude. For the standing acoustic wave it then holds that $|p'_+| = |p'_-| = |p'_{max}|/2$. Furthermore, $\alpha_+ + \alpha_- \approx 2\alpha_0$, with α_0 being the acoustic damping coefficient at quiescent conditions. The following expression is then obtained:

$$\langle P_{vt} \rangle \cong \left[\frac{1}{4} \rho_0 \frac{c_0^2}{c_{eff}} \left(1 - e^{2\alpha_0 L_p} \right) U_b^2 A_p \right] \left(\frac{|p'_{max}|}{\rho_0 c_0 U_b} \right)^2. \tag{9}$$

The acoustic damping coefficient for a smooth pipe (α) is studied extensively in literature (an overview is provided by Weng [27]). α is related to the imaginary part of the complex wavenumber ($\alpha = -Im(k)$). Here, for the wavenumber, the model developed by Dokumaci [28] is used. In the high shear number limit ($sh = \frac{1}{2} D_p \sqrt{\omega_{ac}/\nu} \gg 1$, where ω_{ac} is the angular acoustic frequency, D_p the pipe diameter, and ν the kinematic viscosity), it reads as:

$$k_{\pm} = \frac{\omega_{ac}}{c_0} \frac{\pm \Gamma_0}{1 \pm Ma \Gamma_0}, \tag{10}$$

where $k_{\pm}$ are the complex valued wavenumbers for up- and downstream traveling waves, and $Ma (= U_b/c_0)$ is the Mach number. Γ_0 is a dimensionless wavenumber for sound propagation through a quiescent fluid inside a pipe, taking into account the viscothermal damping only. This model neglects acoustic attenuation by turbulent fluctuations in the bulk of the flow, because the ratio of acoustic boundary layer thickness to thickness of the viscous sublayer of the turbulent mean flow is in the order of one ($\delta^+_{ac} = \delta_{ac}/\delta_l \approx 1$; see Weng [27]). At high shear numbers, Γ_0 can be approximated by Ref. [29]:

$$\Gamma_0 = 1 + \frac{1-i}{sh\sqrt{2}} \left(1 + \frac{\gamma - 1}{\sqrt{Pr}} \right) - \frac{i}{sh^2} \left(1 + \frac{\gamma - 1}{\sqrt{Pr}} - \gamma \frac{\gamma - 1}{2Pr} \right), \tag{11}$$

where Pr is the Prandtl number, the ratio of momentum over thermal diffusivity ($Pr = c_p \mu/\kappa$, with c_p the specific heat capacity, μ the dynamic viscosity and κ the thermal conductivity), and γ is the Poisson constant. An effective pipe length is used for the corrugated pipe section, where the pipe length is adapted using the arc length of the pipe wall in axial direction. This yields increased viscothermal losses for a corrugated pipe (approximately doubled compared to a smooth pipe), comparable to what was found by Belfroid et al. [30].

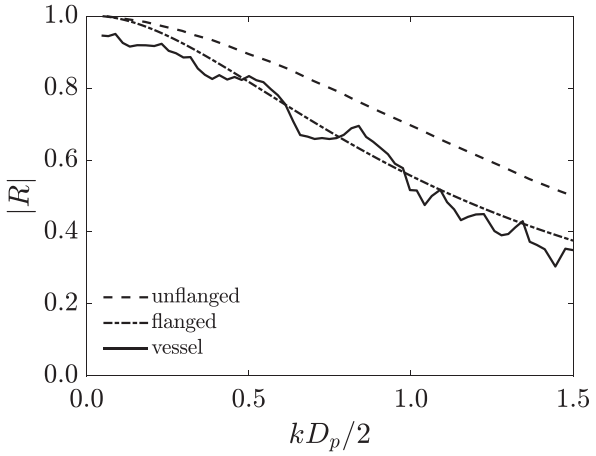

Fig. 1. Experimentally obtained reflection coefficient for the expansion vessel, compared to the reflection coefficient from an unflanged [31] and flanged pipe [32].

3.1.3. Radiation and convection losses

The convective and radiative acoustic losses (second and third right hand side terms in Eq. (4)) at the pipe inlet (towards the expansion chamber) and outlet (flanged open pipe) can be calculated from the acoustic intensity at the respective pipe terminations [33]:

$$\langle P_{\text{rad+conv}} \rangle = A_p \left[\langle I_{in} \rangle + \langle I_{out} \rangle \right]. \tag{12}$$

In this equation, $\langle I_{in} \rangle$ and $\langle I_{out} \rangle$ are the time-averaged acoustic intensities leaving the pipe at the inlet and the outlet, respectively. To obtain these intensities, the acoustic reflection coefficients at the upstream and downstream pipe terminations are required (R_i and R_o). Measurements are carried out to assess the pressure reflection coefficient in the absence of a mean flow for the upstream expansion vessel. A speaker is connected to a smooth steel pipe section (5 mm wall thickness), ending at the expansion vessel. The reflection of the incoming acoustic waves by the vessel is measured using the multiple microphone method [34]. The results are compared to the reflection coefficients for an unflanged pipe [31] and a flanged pipe [32] in Fig. 1. A good agreement is found between the reflection coefficient of the expansion vessel and the flanged pipe, and this relation is therefore used to obtain R_i and R_o. The convective effect of a mean flow on the reflection coefficient is widely studied (e.g. by Ingard and Singhal [35], Davies [36], Munt [37,38] and Peters et al. [39]). For the upstream pipe termination, which is essentially the flow intake, the effect of the mean flow is related to flow separation. Davies [36] studied this configuration and obtained the following estimation for the effect of a mean flow on the pressure reflection coefficient:

$$R_i = R_0((1 - \beta Ma)/(1 + \beta Ma))^{0.9}, \tag{13}$$

where R_0 is the pressure reflection coefficient at quiescent conditions, and β a correction factor to account for additional losses due to flow separation at the sharp-edged inlet. The best fit to experimental data was obtained for $\beta = 1.63$. This expression is combined with the reflection coefficient obtained by Norris and Sheng [32]. For the downstream termination, the effect of the Mach number on the reflection coefficient is taken from Ingard and Singhal [35]. Their result is valid for $kD_p/2 \ll 1$, which does not hold for the present experiments. The reflection coefficient for a flanged pipe in no-flow conditions (by Norris and Sheng [32]) is therefore used. Although Munt [38] showed that the behavior is different for increasing Mach numbers, this difference is rather small for the Mach number range attained in the reported experiments. Moreover, the theory of Munt does not hold for a flanged pipe end, and no literature is available that studies the effect of the Mach number for this case.

$\langle I_{in} \rangle$ and $\langle I_{out} \rangle$ in Eq. (12) are related to the intensities of the acoustic waves traveling inside the pipe:

$$\begin{aligned} \langle I_{in} \rangle &= \langle I^-_{in} \rangle - \langle I^+_{in} \rangle = (1 - R_{E,i}) \langle I^-_{in} \rangle, \qquad \text{and} \\ \langle I_{out} \rangle &= \langle I^+_{out} \rangle - \langle I^-_{out} \rangle = (1 - R_{E,o}) \langle I^+_{out} \rangle, \end{aligned} \tag{14}$$

where $R_{E,i/o}$ are the energy reflection coefficients at the pipe inlet and outlet. These are obtained from the pressure reflection coefficients, according to Ref. [35]:

$$R_{E,i/o} = R^2_{i/o}(1 \pm Ma)^2/(1 \mp Ma)^2. \tag{15}$$

Combining Eqs. (13)–(15) with Eq. (12), and introducing a loss coefficient at the pipe ends ($\alpha_{r,i/o} = 1 - R_{E,i/o}$), results in the following expression for the radiative and convective losses at the inlet and outlet of the pipe:

$$\langle P_{\text{rad+conv, i/o}} \rangle = \left[\frac{1}{2} \alpha_{r,i/o} \rho_0 \frac{c_0^2}{c_{\text{eff}}} U_b^2 A_P \right] \left(\frac{|p'_{-,i/+,o}|}{\rho_0 c_0 U_b} \right)^2. \tag{16}$$

Since the reflection coefficient for higher whistling frequencies is significantly lower than unity, the assumption that $|p'_{\max}| = 2|p^+|$ does not hold at the pipe ends. In crude approximation it takes the form of $|p'_{\max}| = (1 + R_i)|p'_{-,i}|$ at the inlet and $|p'_{\max}| = (1 + R_o)|p'_{+,o}|$ at the outlet. This yields:

$$\langle P_{\text{rad+conv, i/o}} \rangle = \left[\frac{1}{2} \alpha_{r,i/o} \rho_0 \frac{c_0^2}{c_{\text{eff}}} U_b^2 A_P \right] \left(\frac{|p'_{\max}|}{\rho_0 c_0 U_b (1 + R_{i/o})} \right)^2. \tag{17}$$

Combining Eqs. (6), (9) and (17) with Eq. (4), yields a time-averaged power balance, which is used to evaluate whistling in corrugated pipes and to compare it to numerical results. The power balance has the form of

$$A \left(\frac{|p'_{\max}|}{\rho_0 c_0 U_b} \right) = B \left(\frac{|p'_{\max}|^2}{(\rho_0 c_0 U_b)^2} \right), \tag{18}$$

where A and B are parameters related to the flow and fluid properties and the geometry of the system.

3.2. Acoustics of a liquid droplets in a fluid

Injection of liquid into a gas flow inside a pipe increases the acoustic damping. It was shown previously that for corrugated pipes under the studied conditions (annular flow, very low liquid loading) a major fraction of the liquid is present as droplets in the core of the flow, in contrast to smooth pipes where the liquid is mainly transported as a film along the pipe wall [40]. The presence of this dispersed phase causes additional acoustic damping. It is of a viscothermal nature, originating from the viscous and thermal boundary layers occurring at the gas-liquid interface of the droplets. The viscous and thermal effects can in practice be divided into two separate parts [41]:

$$\beta_d = \beta_\tau + \beta_\nu. \tag{19}$$

Here β_d is the viscothermal damping coefficient, due to the presence of droplets. Epstein and Carhart [41] derived an explicit formula for the viscous damping coefficient β_ν, which is valid for acoustically small water droplets ($d_p \ll \lambda_{\text{ac}}$) suspended in an air flow:

$$\beta_\nu = \frac{6\pi d_p}{2c_0} n_d \nu Y_\nu, \tag{20}$$

$$\text{with :} \quad Y_\nu = (1 + z) \frac{16z^4}{16z^4 + 72\delta z^3 + 81\delta^2(1 + 2z + 2z^2)}, \tag{21}$$

$$\text{and :} \quad z = \left(\frac{\omega_{\text{ac}}}{2\nu} \right)^{1/2} d_p/2. \tag{22}$$

For the thermal damping coefficient β_τ, the explicit formula reads:

$$\beta_\tau = \frac{4\pi d_p}{2c_0} n_d (\gamma - 1) \epsilon Y_\tau, \tag{23}$$

$$\text{with :} \quad Y_\tau = 1 + \left(\frac{\omega_{\text{ac}}}{2\epsilon} \right)^{1/2} d_p/2. \tag{24}$$

In these formulations, d_p is the droplet size, n_d the number of droplets per unit pipe length, δ the ratio of the gas and liquid densities, and ϵ the thermal diffusivity. Using the additional viscothermal damping coefficient per unit pipe length (β_d, Eq. (19)), the total acoustic damping due to the presence of droplets is:

$$\langle P_{\text{drop}} \rangle \cong \left[\frac{1}{4} \rho_0 \frac{c_0^2}{c_{\text{eff}}} \left(1 - e^{2\beta_d L_w} \right) U_b^2 A_p \right] \left(\frac{|p'_{\max}|}{\rho_0 c_0 U_b} \right)^2, \tag{25}$$

where L_w is the wetted pipe length, taken as the distance from the liquid injection point to the pipe exit. Combining Eq. (25) with Eq. (18), the total energy balance for the pipe system is:

$$A \left(\frac{|p'_{\max}|}{\rho_0 c_0 U_b} \right) = (B + B_{\text{drop}}) \left(\frac{|p'_{\max}|^2}{(\rho_0 c_0 U_b)^2} \right), \tag{26}$$

where B_{drop} represents the additional damping due to the presence of droplets. To evaluate the droplet damping, it is therefore required to have information on the droplet size distribution and the droplet concentration inside the pipe.

3.3. Howe's theory of vortex sound

Different acoustic analogies have been developed in the past to relate flow properties to sound production. For the studied case, with a solid and stationary body present in a low Mach number flow, two well-known acoustic analogies have been proposed, by Curle [42] and by Howe [43]. Howe's theory of vortex sound [26,43] is a generalization of the acoustic analogy developed by Powell [44] for stationary and rigid bodies in a flow, and uses the total or stagnation enthalpy ($h_t = h + \boldsymbol{u}^2/2$, with h being the specific enthalpy) as acoustic variable. In whistling cavity and corrugated pipe flows (under shear layer mode conditions), the major contributors to the sound production are large coherent vortices, generated in the shear layer spanning the cavities (see the insert in Fig. 2). They dominate over sound production from three-dimensional free turbulence. It is, therefore, intuitive to proceed with Howe's formulation of vortex sound in the present work, because it provides insight into the role of vorticity on the sound production. The energy corollary of Howe defines the time-averaged acoustic source power as follows:

$$\langle P_{\text{source}} \rangle = -\rho_0 \left\langle \int_V (\boldsymbol{\omega} \times \boldsymbol{u}) \cdot \boldsymbol{u}'_{\text{ac}} dV \right\rangle, \tag{27}$$

where V is the volume in which the vorticity $\boldsymbol{\omega}$ is non-vanishing, $\boldsymbol{u}$ is the flow velocity, which is composed of the time-averaged velocity $\boldsymbol{u}_0$ and the hydrodynamic and acoustic fluctuating components ($\boldsymbol{u}'_h$ and $\boldsymbol{u}'_{ac}$, respectively). The source of sound is related to the Coriolis force density $\left(f_c = -\rho_0(\boldsymbol{\omega} \times \boldsymbol{u})\right)$, originating from the interaction of the vortex structures with the acoustic field. Applying a Helmholtz decomposition of the flow field, the acoustic field is defined as a potential velocity field. The acoustic streamlines for a typical cavity geometry are depicted in the insert in Fig. 2, together with a vortex traveling in the cavity mouth. The acoustic source power is obtained numerically using Eq. (27) in the numerical modeling described in Section 7.

4. Experimental

The experiments are carried out in a dedicated open flow loop, where both acoustic measurements and optical measurements are performed. This setup is previously used by the authors, and documented in literature [24,40]. The setup and the different measurement techniques are, therefore, only briefly discussed here.

4.1. Experimental setup

A schematic overview of the setup is provided in Fig. 2. It consists of a blower to provide the air flow, which is followed by an expansion vessel. The vessel both serves to prevent the blower noise to reach the test section and to provide a high reflection acoustic boundary condition for the measurement section, thereby promoting whistling. After the expansion vessel, an acoustic measurement section is placed. The acoustic measurement section is followed by a bend in the pipe (bend radius over pipe radius of approximately 4). Liquid is injected in the vertical part of the setup using a spray nozzle at the pipe centerline. The liquid flow is provided by a rotary vane pump, and the flow rate is measured with a Coriolis mass flow meter. The liquid injection point is followed by a smooth pipe development section, made of steel with a diameter (D_p) of 49.25 mm and a wall thickness of 5 mm. The flow then enters the vertical corrugated pipe, machined from PVC. Several different corrugation geometries are used. They are depicted in Fig. 3 and the geometrical details are listed in Table 1. Geometry A is considered as the base case. It is a generic cavity geometry, and its typical sizing is comparable to many industrially used corrugated pipes. The edges are rounded to enhance whistling, and to resemble industrial applications. The geometries B and C are similar, with only a reduction in the cavity depth and length, respectively. Geometry D is an enlarged version of geometry A, and the geometries E and F are triangular ribs with similar cavity volumes as geometry A. The dimensions for all geometries are listed in Table 1. The total pipe length (L_p) is 3 m for geometries A, B and C, and 3.6 m for geometries D, E and F. The number of cavities (n_c) for all geometries is over 350. For two corrugation geometries (geometry A and D in Table 1) a transparent section (machined from PMMA) with a length of 0.6 m is used for optical access. This section is located towards the end of the corrugated pipe, at $49 \leq L/D_p \leq 53$ for geometry A and at $65 \leq L/D_p \leq 69$ for geometry D. It is contained in a water-filled optical box, to reduce refraction of light at the curved outer pipe wall. The setup ends with an open outflow, blowing into a large room, with no acoustic treatment to the walls. Apart from the measurements described in the following sections, static pressure and temperature measurements are carried out to correct the gas flow rate with the actual gas density. For all measurements, air is used as the gas phase. It is taken from the atmosphere and does not undergo any pre-treatment. The air temperature is close to (atmospheric) room temperature (20 °C). For the liquid injection, two different liquids are used: water and mono-ethylene glycol (MEG). MEG is used for its significantly higher viscosity compared to water (16 times more viscous). Also the surface tension is different for MEG (48 mN/m, compared to 72 mN/m for water). The density of MEG is approximately 10% higher than the density of water [45].

4.2. Acoustic measurements

Four microphones (PCB 106B acoustic pressure sensors) are placed in the acoustic measurement section. The position of the microphones is based on the acoustic frequency range that is expected from the studied corrugated pipes (maximum 3.5 kHz). The spacing between the microphones is based on the work by Jang and Ih [34], and is chosen to be 0.225 m, 0.315 m and 0.360 m

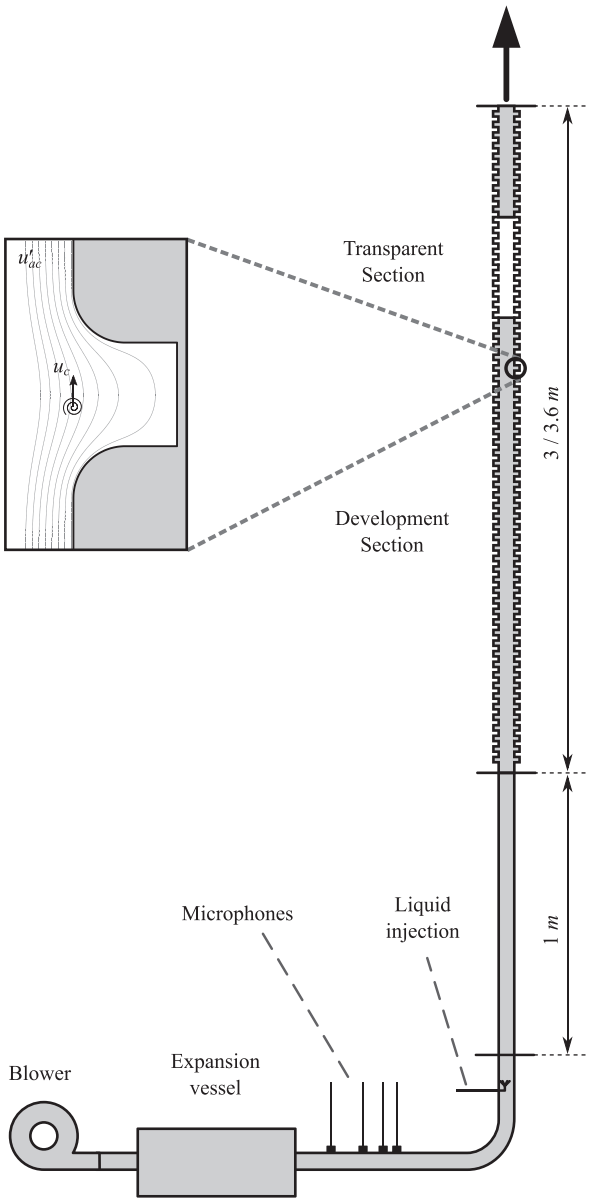

Fig. 2. Schematic representation of the experimental set-up. The gas flow is created by a blower, followed by an expension vessel to prevent the blower noise to reach the test section and to provide a large reflection coefficient boundary condition at the pipe inlet. The flow subsequently enters the acoustic measurement section. Liquid is injected with a spray nozzle at the pipe centerline. The corrugated section is vertical and flow is in upward direction. The corrugated section is partly transparent for the optical measurements. The insert shows a schematic representation of the acoustic streamlines over a cavity structure, with a coherent vortex traveling in the cavity mouth with velocity u_c.

for the second, third and fourth microphone, relative to the first microphone. They are connected to an ICP signal conditioner, and data is recorded with a data acquisition card (National Instruments PCI-4472). The pressure signals are acquired at a rate of 40 kHz, to prevent aliasing from influencing the measurements. Acoustic signals are recorded over a period of 2 s, and repeated four times for every measurement point. The traveling acoustic waves are reconstructed using the multi-microphone method [34]. Subsequently the acoustic amplitude of the standing wave in the pipe is obtained from the traveling waves.

4.3. Liquid cavity filling measurements

The accumulation of liquid between the individual corrugations is measured in the transparent sections of geometry A and D using a *planar laser-induced fluorescence* (PLIF) technique. The technique is similar to PLIF techniques used for film thickness measurements in two-phase annular pipe flow [46], and is previously used for corrugated pipes [24,40]. A fluorescent dye is

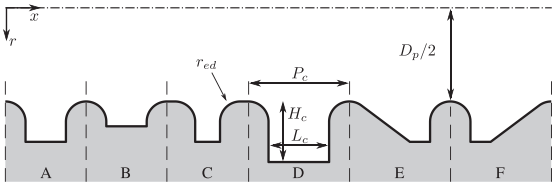

Fig. 3. Schematic representation of the different cavity geometries used in the present study. The cavity size in the figure is exaggerated with respect to the pipe diameter. Definition of the cavity sizes is given in geometry D, values are found in Table 1.

Table 1
Corrugation geometries used in the present study (see Fig. 3). The reference geometry (*ref*) is taken from Nakiboğlu et al. [12] and used is as a benchmark in Section 7. For geometries E and F it is difficult to define the cavity length and depth (indicated with *) due to the slanted cavity bottom.

Geom	A	B	C	D	E/F	ref
L_c (mm)	4	4	2.46	6	*	40
H_c (mm)	4	2.46	4	6	*	27
r_{ed} (mm)	2	2	2	2	2	5
Pt (mm)	8	8	8	10	10	–
L_p (m)	3.0	3.0	3.0	3.6	3.6	–
n_c (–)	374	374	374	359	359	1

added to the injected liquid (rhodamine WT), which is illuminated using a laser. Images are recorded with a CCD camera (LaVision Imager LX 16 M) equipped with a 105-mm Nikkor objective and an optical high-pass filter to only capture the fluorescent light emitted by the liquid at the pipe wall. An example of an image obtained from these experiments is depicted in Fig. 4. The regions where liquid is present are the high intensity regions. The corrugations are indicated in red and the white boundary is obtained after several image processing steps. Note that, due to refraction at the curved pipe wall, liquid cannot be detected accurately on top of the ribs (indicated by the dashed regions in Fig. 4). Only liquid that is attached to the pipe wall can be accurately reconstructed.

4.4. Droplet sizing measurements

The droplet size distribution is obtained using a combination of two different measurement techniques: *interferometric particle imaging* (IPI, Glover et al. [47]) and *shadowgraphic particle imaging* (SPI). Droplet sizes are measured at the pipe outlet, after removal of the liquid film at the pipe wall using a slit [40,48]. The combination of IPI and SPI enables the measurement of a wide range of droplet sizes, up from a few μ*m* in diameter. For a more elaborate description of the droplet sizing measurement technique, the reader is referred to previous work by the authors [40].

5. Dry whistling - experimental

Dry whistling experiments are carried out as a reference to the two-phase experiments that are reported in Section 6 and are briefly discussed here. The whistling frequency shows a step-wise linear increase (as is depicted in Fig. 3 for geometry A). The steps are so-called plateaus in the whistling frequency, caused by the finite number of resonance frequencies of the entire

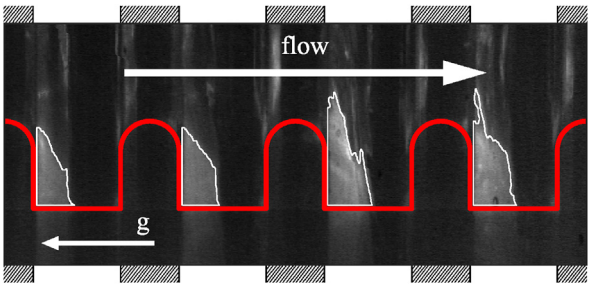

Fig. 4. A typical image obtained from the cavity filling measurements in geometry D. Flow is from left to right, gravity acts in opposite direction. High intensity areas are regions of liquid accumulation. The corrugations are in red, and the detected gas-liquid interface is traced by the white boundary. Liquid on top of the ribs (indicated by the dashed areas) is not detected accurately, due to the curved edges. (For interpretation of the references to color in this figure legend, the reader is referred to the Web version of this article.)

pipe system (see Eq. (2)). The dimensionless whistling amplitude, which is depicted in Fig. 5b, increases with increasing flow velocity up to a Mach number of approximately 0.03. The amplitude slightly decreases for higher flow rates, as a consequence of a reduction in the acoustic reflection coefficient at the pipe ends (see Fig. 1). Within a single frequency plateau, the amplitude peaks in the middle of the plateau, and decreases towards the edges.

Whistling is studied in a range of different cavity geometries, depicted in Fig. 3. Fig. 6a, b and 6c summarize the acoustic behavior for the different geometries. When the cavity depth is decreased (from $H_c/L_c = 1$ for geometry A to $H_c/L_c = 0.615$ for geometry B), the peak whistling Strouhal number decreases from 0.36 to 0.30. A similar behavior was previously observed by, for example, Sarohia [49] for a different cavity geometry. The effect was attributed to a reduced convection velocity of vortices in the cavity mouth, as a result of the vortex-wall interaction [12]. When the cavity bottom is in closer proximity to the shear layer, the interaction with the wall strengthens. The whistling amplitude also slightly decreases, due to the changed shear layer behavior. Whistling still occurs over the entire Mach number range covered by the experiments, and the onset velocity remains unchanged.

The corrugated pipe with narrow cavities (geometry C, $H_c/L_c = 1.626$) shows delayed onset of whistling at $Ma = 0.08$ (Fig. 6c). The is caused by the longer plateau between the cavities, and the shorter shear layer region over the cavities. The boundary layer growth over the plateau results in a thicker and more stable incoming boundary layer [13]. The spatial extent of the cavity mouth, which is the region of sound productions, is also smaller for geometry C, resulting in a lower whistling amplitude. The longer effective smooth pipe length causes a further reduction of the amplitude, by adding viscosthermal damping to the system.

Whistling in a corrugated pipe with geometry D, which is enlarged by 50%, follows the same trend as whistling in geometry A. The whistling amplitude is, however, significantly larger, and the decrease in amplitude at the higher Mach number range is not as strong. This is caused by a relative increase of the source region size per unit pipe length, yielding an increased acoustic amplitude. The importance of end effects is also reduced due to the larger pipe length. The increased cavity depth results in a small increase of the whistling Strouhal number, due to the reduced vortex-wall interaction for this geometry.For the triangular corrugation geometries (geometries E and F) whistling is only observed when the slanted edge is at the upstream side of the cavity. The acoustic field is altered, and the acoustic streamlines at the downstream cavity side are more aligned with the convection direction of the vortices for geometry F. Knowing that the source of sound is related to $(\boldsymbol{\omega} \times \boldsymbol{u}) \cdot \boldsymbol{u}'_{\mathrm{ac}}$ (as explained in Section 3.3) this causes a decrease of the amplitude of sound production, which is largely located at the downstream cavity edge as will be shown in Section 7.3. This effect is strengthened because vortices inside the shear layer are ejected from the cavity mouth more easily [50]. Geometry E shows whistling over the entire Mach number range. Absorption at the upstream edge is decreased, compared to geometry F. The whistling Strouhal number is in the same range as was obtained for geometry A. The whistling amplitude is rather low, compared to the other geometries. It is expected that the confinement plays a significant role in the upstream half of the cavity. Cavity E seems to behave like a shallow version of cavity geometry D.

5.1. Energy balance model

Due to differences in the pipe length, the number of corrugations and the whistling frequency, it is difficult to quantitatively compare whistling in the different corrugation geometries using the acoustic pressure only. The acoustic losses for the different pipes are not the same, and also depend on the whistling frequency and amplitude. To be able to compare the whistling amplitude in a more quantitative way, an *energy balance model* (EBM, described in Section 3.1) is used. The experimental data are used as input (whistling amplitude and frequency, bulk flow velocity, temperature, pressure, system geometry, etc.), and the

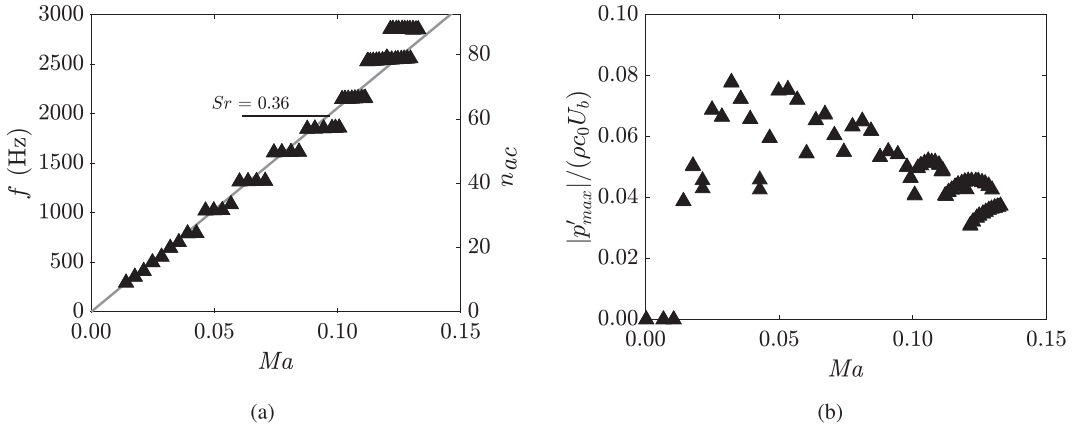

Fig. 5. (a) Whistling frequency (f) as a function of the Mach number for geometry A, showing the step-wise increase in whistling frequency. The solid line represents $Sr = 0.36$. The right hand side y-axis shows the acoustic resonance mode n_{ac} of the pipe system (see Eq. (2)), associated to the whistling frequency. (b) Dimensionless amplitude of the acoustic standing wave ($|p'_{max}|/(\rho_0 c_0 U_b)$) as a function of the Mach number for geometry A.

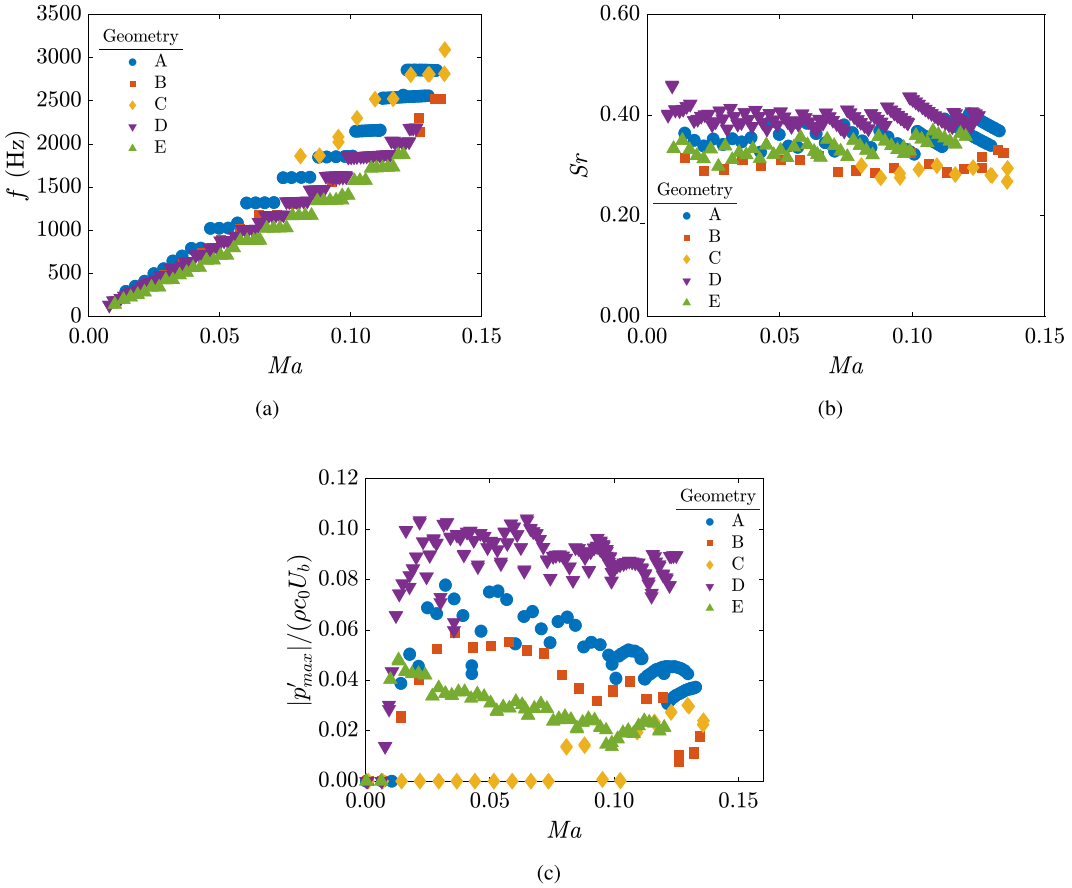

Fig. 6. Whistling frequency, whistling Strouhal number and amplitude as a function of the Mach number, for the geometries depicted in Fig. 3. (b) Whistling Strouhal number as a function of the Mach number, for the geometries depicted in Fig. 3. (c) Dimensionless acoustic amplitude as a function of the Mach number, for the geometries depicted in Fig. 3.

acoustic losses are estimated at the operating conditions. The visco-thermal, and radiative and convective losses are calculated according to Eqs. (9) and (17), respectively. Knowing that under whistling conditions the time-averaged acoustic losses must balance the production of acoustic power, the required acoustic source strength can be obtained. This total source strength is divided by the number of corrugations present in the respective corrugated pipe, and the results are listed in Table 2 for the different corrugation geometries. The reported values are obtained at a gas flow velocity of 40 m/s, for which all geometries, apart from geometry F, exhibit whistling in the experiments. The viscothermal losses make up between 45 and 55% of the total acoustic losses for the different corrugated pipes.

The obtained trend underlines the geometrical properties that determine the acoustic source strength of a specific corrugation geometry. The effect of the cavity length on the source strength is evident comparing geometries D, A, and C. Shorter cavities display a reduced source power, due to the reduction of the size of the source region. The difference in source power between geometry A and B is caused by the interaction with the cavity bottom that comes into play for shallower cavities. This is also expected to play an important role for geometry E. The slanted bottom at the upstream side of the cavity limits the growth of vortices in the shear layer, causing a strong reduction in source power for this geometry. This effect, however, requires further study of the flow field. The edge rounding, mainly for the upstream edge, is an important parameter for the whistling amplitude.

Table 2
Experimentally obtained peak whistling Strouhal number and normalized acoustic source strength P_s for the different corrugation geometries studied, at $U_b = 40$ m/s. The energy balance model, described in Section 3, is used to estimate the acoustic losses in the system, resulting in the source strength values.

Geometry	A	B	C	D	E
Sr_{pw} (−)	0.36	0.30	0.28	0.41	0.35
$\langle P_s \rangle / (\rho U^2 A_p \lvert u'_{ac} \rvert) (\times 10^{-3})$	0.83	0.48	0.40	1.60	0.35

With the experimentally studied geometries, however, it is difficult to quantitatively evaluate the impact of edge rounding on the whistling strength.

6. Liquid addition - experimental

When a liquid is added to the pipe flow upstream of the corrugated section the whistling amplitude is significantly reduced. This is depicted in Fig. 7a for water addition to air flow through a pipe with geometry A (see Table 1 and Fig. 3 for geometrical details). The results are similar to previous work for this geometry [24]. A linear reduction of the acoustic amplitude with liquid volume fraction φ_l (defined as the ratio of the liquid volume flow rate over the gas volume flow rate) in the pipe is observed, as was previously found for this geometry [24]. A very small liquid fraction is sufficient to entirely suppress whistling in this geometry and this critical φ_l increases with increasing gas flow velocity. Experiments in a corrugated pipe with geometry D show the same linear relation between acoustic amplitude and the amount of liquid added to the pipe flow (Fig. 7b).

The effect of the gas flow rate is, however, less evident. The highest flow velocity still requires the largest liquid fraction to mitigate whistling entirely. For lower values of φ_l, however, the largest whistling amplitude is not always observed for the largest flow speed. Especially for $U_b = 35$ m/s and 42 m/s, the whistling amplitude at the lower φ_l range is considerably smaller compared to the other flow velocities. For these cases the lock-in between the acoustic standing wave and the cavity vortex shedding is less strong. There is a significant difference in the amount of liquid required to mitigate whistling entirely for geometry A and D. As a consequence of the larger cavity size, more liquid is required to cause a considerable reduction in acoustic output. The higher acoustic source power for this geometry in single phase conditions (see Fig. 6c) also causes more acoustic damping or a greater source power reduction required to diminish whistling.

For the other studied geometries that showed whistling in dry conditions (geometries B, C and E), only geometry C and E still produce sound when liquid is added (see Fig. 8). The pipe with the shallow cavities of geometry B remains silent. The short cavity of geometry C only whistles for the highest gas flow velocity (42 m/s) and at very low liquid volume fractions. This also holds for the pipe with triangular cavities (geometry E): no whistling is observed for any gas flow velocity for $\varphi_l > 1.5 \times 10^{-5}$.

To assess the effect of liquid properties on the whistling behavior, mono-ethylene glycol (MEG) is added to the dry gas flow instead of water. Results are depicted in Fig. 9a and b. When MEG is added to the flow instead of water, the required liquid flow rate for whistling mitigation is slightly increased. Only the result for the highest Mach number in geometry D ($Ma = 0.117$) deviates from the results with water injection. The whistling amplitude at this Mach number significantly lower for MEG injection, compared to water injection. Whistling under these conditions occurs at an increased frequency compared to whistling with water injection. The MEG injection causes mode switching to a different acoustic pipe mode, resulting in changes in acoustic boundary conditions and hence, changes in acoustic whistling amplitude. Comparison of Fig. 9 with Fig. 7 shows that it is unlikely that the viscosity of the used liquid, which is 16 times higher for MEG, has a significant effect on the resulting whistling mitigation behavior.

6.1. Acoustic droplet damping

Droplet size measurements are carried out for geometry A to assess the droplet size distribution and its effect on the acoustics of the entire pipe system. To illustrate the potential effect of droplets on the acoustics, the case at a gas flow velocity of 42 m/s and with a liquid loading just beyond whistling (liquid flow rate of 305 mL/min, $\varphi_l = 6.2 \times 10^{-5}$) is used as an example. More details on the droplet size distribution can be found in Ref. [40]. The accompanied additional acoustic damping coefficient is calculated according to Eqs. (19 - 24). It is assumed that all injected liquid is present as a dispersed phase in the bulk of

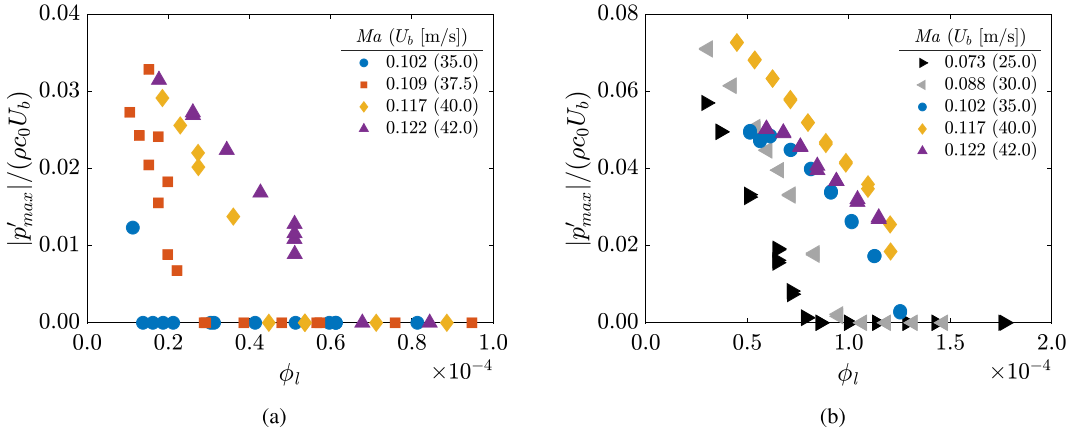

Fig. 7. Dimensionless acoustic whistling amplitude as a function of the liquid volume fraction φ_l for pipes with a reference corrugation geometry A (a) and the enlarged geometry D (b, see Fig. 3).

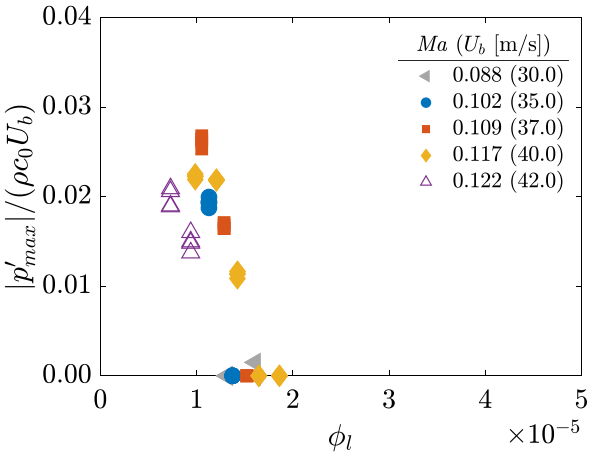

Fig. 8. Dimensionless acoustic whistling amplitude as a function of the liquid volume fraction φ_l for corrugated pipes with geometry C (open markers) and E (closed markers).

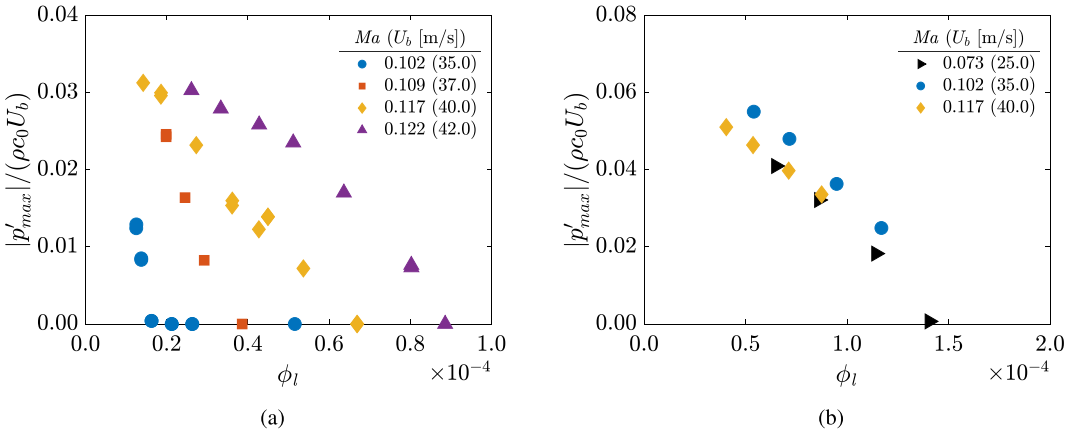

Fig. 9. Dimensionless acoustic whistling amplitude as a function of the liquid volume fraction φ_l for corrugated pipes with geometry A (a) and D (b). Mono-ethylene glycol (MEG) is used in these measurements, instead of water (compare to Fig. 7).

the pipe flow, and that no liquid is present at the walls. From previous work it is known that the actual amount of entrained liquid approaches full entrainment for corrugated pipes. The liquid entrainment ratio at the studied conditions is approximately 0.9 [40]. Assuming full entrainment, therefore, results in a slight overestimation of the acoustic damping by the presence of droplets. The total acoustic damping coefficient per unit pipe length due to the presence of droplets for this case amounts $\approx 3.5 \times 10^{-5}$ m^{-1}. Assuming that the source power is unaffected by the presence of droplets, these additional acoustic losses cause a reduction of the fluctuation amplitude by approximately 0.01%. In the experiments, however, this volume fraction of liquid already caused total whistling mitigation. The presence of droplets is therefore not likely to play an important role in the reduction of the acoustic output from corrugated pipes. The interaction of droplets with the shear layers spanning the individual corrugations, however, might still be an important factor.

6.2. Cavity filling

The filling of cavities with liquid is important for whistling mitigation in corrugated pipes [24]. The liquid filling acts as a solid wall for the gas flow, as a consequence of the large difference in typical time-scales in the two phases, and changes the geometry of the corrugations. In previous work, geometry A was used, and water filling was assessed only. Those experiments are extended here towards an enlarged geometry (geometry D) and to a different working fluid (MEG). The filling profile is measured using laser-induced fluorescence measurements, as described in Section 4. The filling is expressed as the fraction of the cavity volume filled with liquid, averaged in time and over several cavities (α).

Fig. 10a shows the decreasing acoustic amplitude as a function of α, for two-phase water-air flow through a corrugated pipe with geometry A. The results for different gas flow velocities collapse and are in good agreement with previous measurements in the same geometry [24]. Fig. 10b shows results for MEG-injection in the same geometry. The general behavior closely resembles

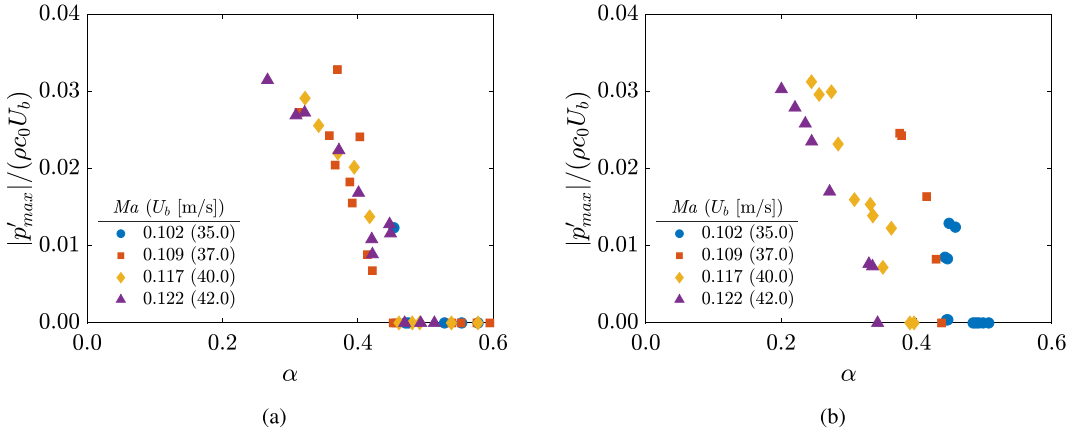

Fig. 10. Dimensionless whistling amplitude as a function of the liquid filling fraction α, for geometry A with water (a) and MEG (b) injection.

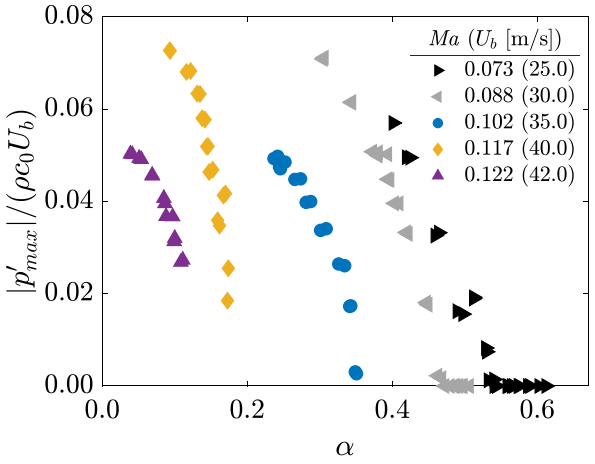

Fig. 11. Dimensionless whistling amplitude as a function of the liquid filling fraction α, for geometry D, with water injection.

that of water-air flow. Compared to Fig. 10a a slightly larger spread is observed as a function of the gas flow rate. For a pipe with the enlarged corrugation geometry D the behavior is different (Fig. 11). The whistling amplitude still decreases with an increase in the liquid filling fraction α. There is, however, a strong influence of the gas flow velocity on this trend. The filling fraction required to prevent whistling ranges from 0.2 to 0.5. An increase in gas flow rate results in a lower α required to fully mitigate whistling. It has to be noted that the range of bulk gas flow velocities is considerably larger compared to geometry A. The required liquid volume fraction φ_l to silence this geometry at the highest gas flow rate could not be reached in the present setup.

The liquid fill fraction is a global parameter and does not properly describe the relevant geometrical changes to the cavities that cause reduction of the acoustic output. To gain more insight in the effect of liquid filling, the filling profiles are plotted in Fig. 12a, b and 12c. The profiles displayed represent different gas flow rates, at the point where whistling has just disappeared. A significant difference is observed in the effect of the gas flow rate on the filling profiles for the studied cases. For the base case (geometry A, water addition), the differences between the profiles are limited, and only occur through a change in effective, or empty cavity depth at the upstream side of the cavity. For the larger corrugation geometry (geometry D), there is a more significant change, mainly exhibited through a shortening of the empty cavity length. When switching to MEG, a similar behavior is observed, where the empty cavity length is reduced when the gas flow velocity increases.

Apart from the geometrical alterations to the cavity geometry and the acoustic damping due to droplets, additional acoustic damping due to liquid at the pipe wall and the shear-layer disruption by liquid could also lead to a reduction in acoustic amplitude. To investigate this, a corrugated pipe is produced, with a cavity geometry based on the liquid profiles discussed in this section. The liquid profile that was measured in the pipe with geometry A, at a gas flow velocity of 40 m/s, just beyond the point where whistling disappears is used. A pipe is machined with the same length and number of cavities as geometry A, the only difference being the altered cavity geometry. The acoustic output of this pipe is measured over a range of flow settings. No whistling occurred over the entire flow velocity range possible in the experimental setup. This strengthens the conclusion that

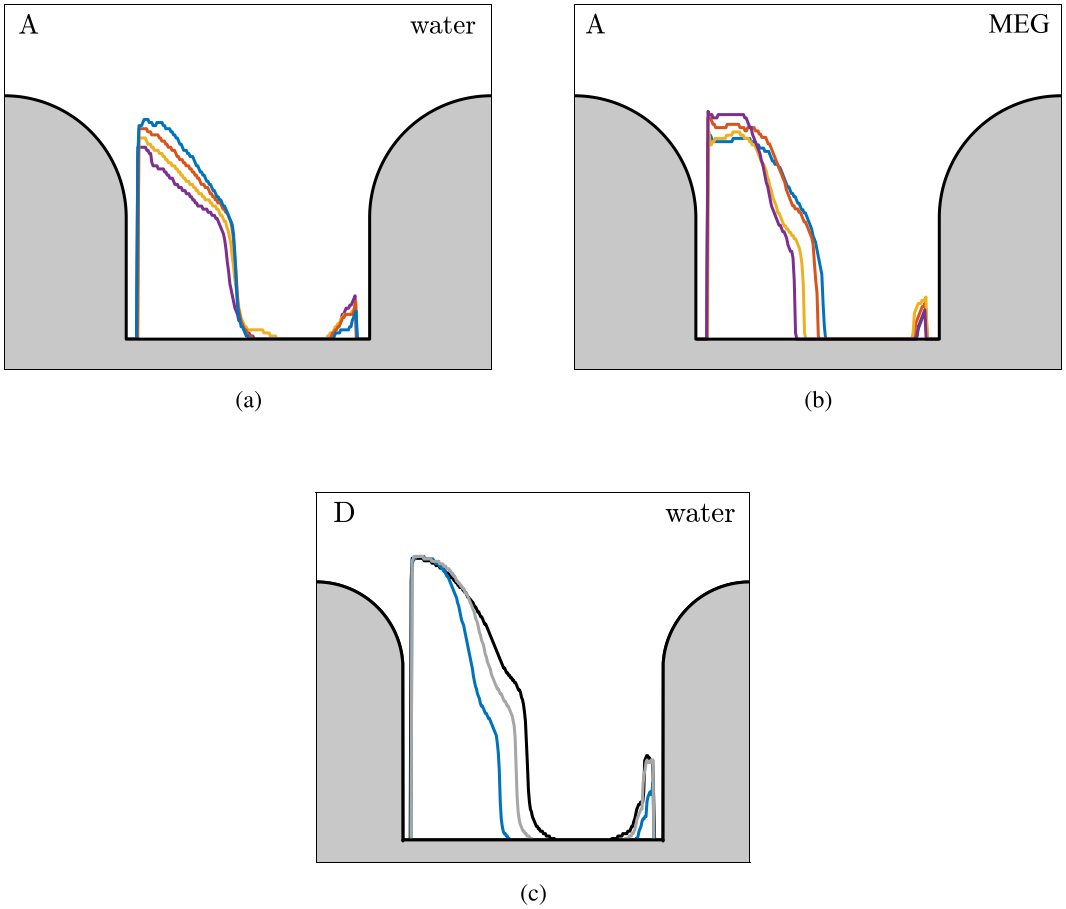

Fig. 12. Averaged liquid filling profiles for geometry A with water injection (a) and MEG injection (b) and for geometry D with water injection (c). The profiles are for liquid flow rates where whistling has just disappeared. The colors correspond to the colors used in Fig. 10a, b, and 11, respectively. (For interpretation of the references to color in this figure legend, the reader is referred to the Web version of this article.)

indeed the alteration of the cavity geometry is the main source of whistling mitigation.

The cavity filling mechanism also explains the limited amount of liquid required to silence pipes with geometries B, C and E. The reduced dry whistling amplitude and the smaller cavity volume together result in a smaller liquid fraction required to mitigate whistling, compared to geometry A. For geometry E, however, another effect appears concurrently, as will be shown in Section 6.3.

Several distinct geometrical alterations are expected to play a role when it comes to the reduction of the acoustic amplitude. The three most important are: (1) a shortening of the cavity shear layer, (2) a change of the upstream cavity edge geometry and (3) an alteration to the deeper part of the cavity. When the shear layer region becomes shorter, a reduction in the spatial extent of the acoustic source region results in lower acoustic amplitudes. It is also known from literature that rounding of the upstream edge has a strong effect on the acoustic amplitude [5,10]. For a sharper upstream edge, the stronger local directional change of the acoustic streamlines at the flow separation point will cause a stronger acoustic absorption at the upstream cavity wall, and hence, a lower acoustic output. Since the liquid acts as a solid wall from the perspective of the gas flow, the presence of liquid at the ribs and the flow separation point will lead to different acoustic outputs. This can, however, not be studied from the experimental results. Adaptions of the deeper part of the cavities will affect the recirculation zone that is present beneath the shear layer. Because of the interaction between the shear layer dynamics and the recirculation zone this might influence the vortex shedding and growth rate, and thereby the acoustics. It is expected that this effect will only occur for shallower cavities (as is shown by Ref. [12]). These effects will be further studied through simulations in the second part of this work (see Section 7).

6.3. Axisymmetry of filling

A non-axisymmetryic filling can lead to a reduced acoustic output ([20]). For geometry D, after manufacturing, the pipe wall was covered with oil, resulting in a hydrophobic internal surface. When this pipe is subsequently subjected to an air-water

flow, the axisymmetry of the filling is broken (Fig. 13a) Small patches of liquid appear at the inner cavity wall and the liquid accumulation shows a reduced azimuthal regularity. A similar filling behavior is observed for two-phase flow through a pipe with corrugation geometry E, where the absence of an upstream rectangular inner cavity corner hinders liquid accumulation inside the cavities. The acoustics generated by a pipe in this flow regime are quite different compared to the axisymmetric regime discussed in the previous sections. Fig. 13b shows the acoustic amplitude as a function of the liquid volume fraction for the two regimes in geometry D, at a superficial gas velocity of 42 m/s. When the filling is non-axisymmetric in nature, whistling disappears at a substantially lower liquid volume fraction. Irregularities in the corrugation geometry in azimuthal direction can break the coherent nature of the vortex shedding. This process appears to be more effective in whistling mitigation, than the mere filling of the cavities. Wall-treatment of the pipe resulting in a large contact angle with the working liquid would, therefore, cause a reduction in the required amount of liquid for whistling to disappear. Cavity geometries preventing the formation of an azimuthally continuous liquid filling (like geometry E) is expected to have a similar effect. Further experiments should be carried out to confirm this.

7. Whistling in corrugated pipes - numerical

Although qualitative and quantitative information is obtained from the whistling experiments in different geometries, many factors are still intertwined and remain unclear. Without flow-field information, it is difficult to distinguish between the effect of the cavity geometry on the source and other effects such as the global acoustical properties of the system. Furthermore, the effect of changes to specific parts of the cavity geometry cannot be identified easily from the experiments. To isolate the acoustic source power and to investigate which specific parts of the geometry play an important role, a numerical model solution is used. This method is based on the work by Martínez-Lera et al. [9], Nakiboğlu et al. [10] and Golliard et al. [51]. The validity of the method is first assessed, after which an modification is proposed that provides more insight in the whistling cycle in corrugated pipes.

The numerical method is based on incompressible flow simulations. The main flow structures that are responsible for the sound generation are the vortices shed in the cavity mouth. These large flow features can be captured in an incompressible, 2D-axisymmetric simulation. Since acoustics cannot exist in incompressible simulations, an acoustic analogy is applied to obtain the acoustic power generated by the flow through a certain geometry. The shedding of vortices is triggered by superimposing a fluctuating component to the incoming velocity profile. It is applied at the pipe inlet, located 2 mm upstream of the leading cavity edge. A uniform perturbation amplitude is used, as the acoustic boundary layers are typically very small (of the order of the viscous sublayer). This fluctuating velocity perturbation mimics the acoustic standing wave that develops in real corrugated pipes and that synchronizes vortex shedding in the individual shear layers. A single cavity in a pipe is modeled, omitting the interference effect between subsequent cavities. Fig. 14 shows the numerical domain used in the simulations, in this case for geometry A (see Fig. 3). The cavity zone is densely meshed, especially near the cavity mouth. Grid sizes reduce towards the wall, where a y^+ value around 1 is maintained. The total number of quadrilateral cells ranges from 55,000 to 77,000, depending on the cavity geometry. A grid dependence study showed little differences for higher numbers of grid cells (up to over 200,000).

7.1. Numerical method

As a starting point for the calculation of the acoustic source power, Howe's theory of vortex sound is used [4]. This theory is derived from Crocco's momentum equation. For a homentropic flow, ignoring viscous contributions to the flow (valid for high

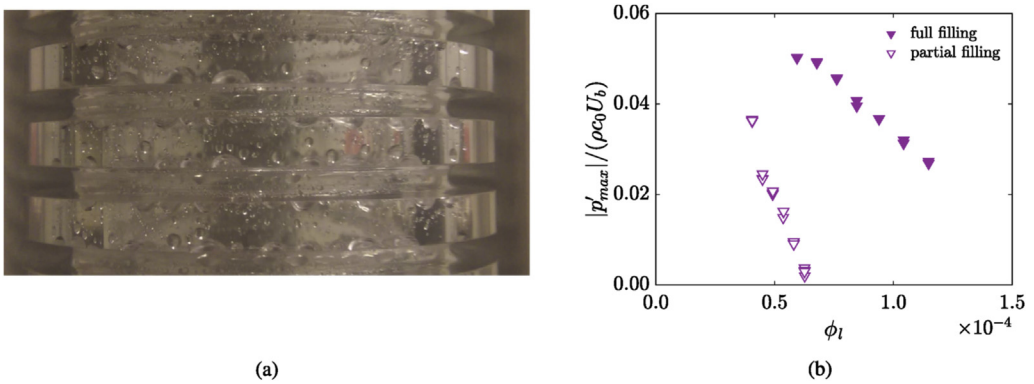

Fig. 13. (a) Qualitative view of the filling pattern for a corrugated pipe with geometry D after hydrophobic wall treatment. (b) Dimensionless whistling amplitude as a function of the liquid volume fraction, for two-phase water-air flow through a pipe with corrugation geometry D. When the axisymmetry of the filling is broken due to a non water-wetting coating of the wall (open markers), the required liquid volume fraction to make whistling disappear is substantially reduced.

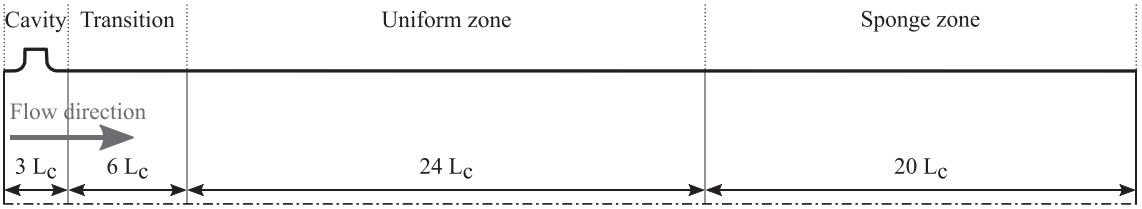

Fig. 14. Numerical domain used for simulations of the cavity with geometry A. The cavity zone is densely meshed, followed by a transition to a uniform grid size. The sponge zone is applied to reduce reflections from the outlet.

Reynolds numbers), Crocco's equation is written as:

$$\nabla h_t = -\frac{\partial \boldsymbol{u}}{\partial t} - (\boldsymbol{\omega} \times \boldsymbol{u}), \tag{28}$$

where h_t is the stagnation enthalpy and $\boldsymbol{\omega}$ the vorticity. Combining this equation with Howe's energy corollary (see Eq. (27)), yields an equation for the acoustic source power:

$$\langle P_{\text{source}} \rangle = -\rho \left\langle \int_V (\boldsymbol{\omega} \times \boldsymbol{u}) \cdot \boldsymbol{u}'_{\text{ac}} dV \right\rangle, \tag{29}$$

$$= \rho \left\langle \int_V \nabla h'_t \cdot \boldsymbol{u}'_{\text{ac}} dV \right\rangle + \rho \left\langle \int_V \frac{\partial \boldsymbol{u}}{\partial t} \boldsymbol{u}'_{\text{ac}} dV \right\rangle. \tag{30}$$

In this equation, h'_t is the fluctuating part of the total enthalpy. The second right hand side term of Eq. (30) is neglected. The validity of this assumption will be checked in Section 7.2. Applying the divergence theorem, knowing that $\nabla \cdot \boldsymbol{u'_{ac}}$ is negligible in a compact source region, results in a formulation of the acoustic source power related to the fluctuating total enthalpy:

$$\langle P_{\text{source}} \rangle = \rho \left\langle \int_S (h'_t \boldsymbol{u}'_{\text{ac}}) \cdot \vec{n} dS \right\rangle. \tag{31}$$

By choosing a large control surface, ensuring that hydrodynamic fluctuations are insignificant at the downstream boundary, the second right hand side term of Eq. (30) can indeed be neglected [10]. The large control surface, however, also contains a significant smooth pipe length where the effect of the cavity is reduced by viscous dissipation. To isolate the source power, a smooth pipe reference case is subtracted from the obtained result:

$$\langle P_s \rangle = \langle P_{\text{source}} \rangle - \langle P_{\text{smooth}} \rangle, \tag{32}$$

where P_s is the corrected source power. It is claimed that using this method the effect of the Reynolds number on the acoustic source power is removed, enabling the use of lower Reynolds number simulations for a higher Reynolds number case [10]. The acoustic source power was overestimated by approximately a factor 2 with this method. Later, Golliard et al. [51] carried out a URANS simulation, which extends the applicability of the method to higher Reynolds numbers due to a better representation of the shear layer growth in the cavity region. They claim a significant increase in accuracy of the predicted source power to within 20% of the experimental results.

Instead of using the total enthalpy to obtain the acoustic source power, one can also directly apply Eq. (29). In that case no smooth pipe reference simulation is required. The only additional demand is that the local distribution of the acoustic velocity field at the location of the cavity is known. Bearing in mind that the acoustic velocity corresponds to the unsteady potential component of the flow, a separate potential flow simulation is performed to obtain the distribution of $\boldsymbol{u}'_{\text{ac}}$. Assuming that the local acoustic field is not significantly altered by the flow, which is expected to be valid for low Mach numbers and checked in Section 7.2, it is subsequently combined with the incompressible URANS simulation of the cavity geometry to obtain the source power. The advantage of this method, apart from omitting the need for a reference simulation, is that it provides insight in the local spatial distribution and temporal evolution of regions of production and absorption of acoustic energy in the cavity. It therefore adds to understanding the effect of specific geometrical cavity alterations to the acoustic output of a certain corrugation geometry. In the following the two methods will be compared to literature and to each other, after which they are applied to the different corrugation geometries studied in the present work. The two methods are referred to as the *vorticity* (Eq. (29)) and the *enthalpy* (Eq. (31)) method respectively.

7.2. Comparison of the two methods

To assess the difference between the two methods, the geometry studied by Nakiboğlu et al. [12] and Golliard et al. [51] is used as a benchmark case. This cavity has a length of 40 mm and a depth of 27 mm, and is placed inside a pipe with a diameter

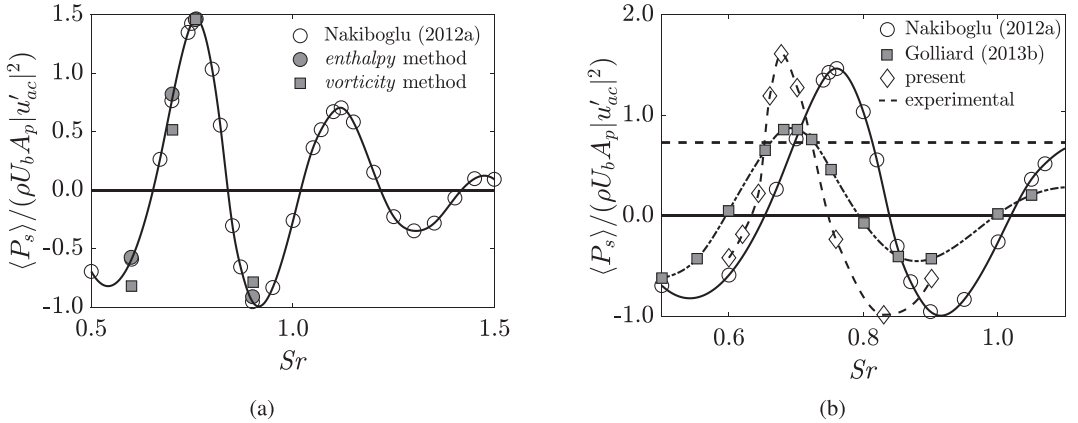

Fig. 15. (a) Comparison of the dimensionless acoustic source power as a function of the whistling Strouhal number obtained with the *enthalpy* and *vorticity* method, compared to results from literature [12,51] at a Reynolds number of 4×10^3 (a) and 4×10^4 (b). The experimentally obtained source power, depicted in (b), is also taken from Nakiboğlu et al. [12].

of 44 mm. The cavity edges are rounded and have a radius of 5 mm. Gas phase Reynolds numbers based on the pipe diameter of 4×10^3 and 4×10^4 are used.

The inlet velocity profile is obtained from Nakiboğlu et al. [12] and a moderate perturbation amplitude of $|u'|/U_b = 0.05$ is used.The results from Nakiboğlu et al. [12] are accurately reproduced by both methods (as is depicted in Fig. 15b). That the *enthalpy* and *vorticity* methods lead to similar results shows that the second right hand side term in Eq. (30) is indeed negligible. It also proves that the assumption that the acoustic field can be decoupled from the flow field as is done in the *vorticity* method.

For the higher Reynolds number case ($\mathrm{Re} = 4 \times 10^4$) the URANS method (with a $k - \omega$ turbulence model, as was used by Golliard et al. [51]) is applied, and the results are compared to results obtained by Golliard et al. [51] in Fig. 15b. There is a good agreement with respect to the whistling Strouhal number, however, the obtained source power is almost a factor 2 higher than the value that is reported by Golliard et al. It is most likely that a difference in perturbation amplitude in the simulations is causing the discrepancy, since only the obtained source power is different. Golliard et al. [51] do not explicitly mention the perturbation amplitude that was used in their study. For the present study a perturbation amplitude of 5% of the bulk velocity is used which is close to the experimental value. For a perturbation amplitude of $|u'|/U_b = 0.10$, a close match between the present method and the results reported by Golliard et al. [51] is obtained, suggesting that this is the perturbation amplitude that was used in their study.

Both methods are used to assess the source power in geometry A and D (see Fig. 3). The amplitude of the source power obtained with the *vorticity* method is always within 8% of that of the *enthalpy* method. Differences in the whistling Strouhal number are even smaller. Using Howe's energy corollary directly has several advantages: it gives direct insight in the temporal and spatial evolution of the acoustic source power, and it omits the requirement of a reference flow calculation and hence, reduces computational demands. This method is therefore used in all the cases considered in the following.

7.3. Reference case geometry A

The cavity geometry A is used as a reference case to evaluate the accuracy of the URANS simulation compared to acoustic data from experiments. The gas flow velocity is taken as 40 m/s and the incoming velocity profile for this geometry is obtained from a separate periodic URANS simulation in a corrugated pipe without a velocity perturbation at the inlet. The resulting velocity profile closely resembles a power law profile, with a power of 4.8 [52], which is used as the inlet velocity profile for all simulations. The time-averaged acoustic source strength $\langle P_s \rangle$ is obtained over a range of whistling Strouhal numbers by changing the oscillation frequency of the velocity perturbation. The results are depicted in Fig. 16a. When $\langle P_s \rangle$ is positive, sound may be produced. Two peaks are observed, indicating the second and third hydrodynamic modes. The second mode is dominant, while the third mode barely produces any acoustic energy. The amplitude of sound production depends on the acoustic losses present in the system. Sound will be produced when the time-averaged acoustic source power exceeds the acoustic losses of the system.

7.3.1. Whistling cycle

The temporal variation of the source strength over a single whistling cycle is depicted in Fig. 16b. Two peaks in the source strength occur, related to the minimum and maximum acoustic velocity during an oscillation period. Both peaks are positive due to the sign change of the acoustic field at $t/T = 0.5$. Vortex formation in the shear layer is initiated when the acoustic velocity switches direction, from negative to positive x-direction [8,53]. This point is indicated by A in Fig. 16b. At this instance the preceding vortex is present half-way the cavity (as is depicted in Fig. 17a). The associated source power (Fig. 17b) is low

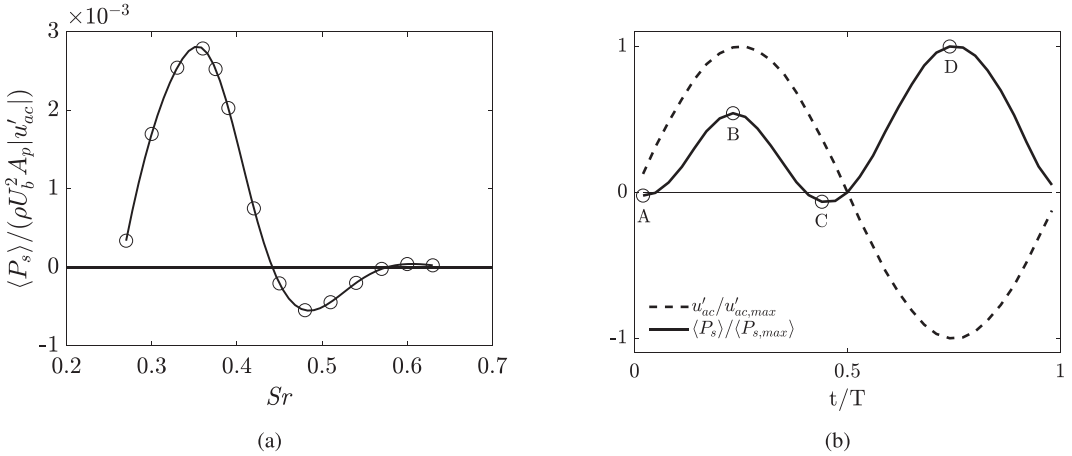

Fig. 16. (a) Dimensionless acoustic source power as a function of whistling Strouhal number for geometry A, at a perturbation amplitude of $|u'_{ac}|/U_b = 0.1$, and a bulk velocity of 40 m/s. (b) Temporal distribution of the source strength (–) and the acoustic perturbation amplitude (–) over a full period of the perturbation cycle at the peak-whistling Strouhal number. The bulk gas velocity is 40 m/s, the perturbation amplitude amounts 10% of the bulk velocity. Values are normalized with the maximum values obtained in a whistling period. The points A, B, C and D relate to Fig. 17.

due to the vicinity of the zero acoustic velocity point ($u'_{ac} \approx 0$). Sound is subsequently produced at the downstream cavity edge when the vortex is convected further downstream (Fig. 17c and d, B in Fig. 16b). Acoustic absorption occurs at the upstream edge simultaneously, caused by the newly generated vortex. When the spatially averaged acoustic source power becomes negative (C in Fig. 16b) the absorption region near the upstream edge is growing, whereas production from the downstream vortex shrinks due to its ejection from the cavity (Fig. 17e and f). The largest instantaneous source power is observed when the acoustic particle velocity is at its negative peak (D in Fig. 16b). Production then occurs in the upstream half of the cavity, as a result of the directional change of the acoustic velocity (see Fig. 17g and h).

Averaging of the instantaneous source power over several whistling cycles results in the spatial distribution of absorption and production regions over the cavity. Fig. 18a shows this spatial distribution for geometry A, at a bulk velocity of 40 m/s and a perturbation amplitude of $|u'_{ac}|/U_b = 0.1$. Acoustic power is mainly produced near the downstream edge and at approximately a quarter of the cavity length. The major absorption region is located at the upstream edge, as expected from literature. All significant absorption and production takes place inside the shear layer region; the deeper parts of the cavity do not contribute much to the sound production. It is therefore expected that the internal cavity geometry is not of great direct influence to the acoustic output. Only through a possible change in the shear layer behavior it might affect the sound production, which occurs for shallow cavities. The main geometrical cavity properties that determine the acoustic amplitude (apart from the acoustic properties of the pipe system) are the size of the cavity mouth and the geometry of the cavity edges, particularly of the upstream edge.

7.3.2. Scaling of source power

As discussed in Section 3, the source strength behavior strongly depends on the perturbation amplitude $|u'_{ac}|/U_b$. From Eq. (27) it is expected that the net acoustic source power scales with the bulk velocity squared and with the acoustic perturbation velocity, but this only holds when the vorticity in the shear layer is fully concentrated in discrete vortices that convect downstream towards the cavity edge. To evaluate these scaling arguments, simulations are performed at different perturbation amplitudes in geometry A. The effect of the bulk velocity (or the Reynolds number) is also assessed. Fig. 19a shows the dimensionless source strength as a function of U_b. A reduction of the bulk velocity from 40 to 10 m/s causes a 30% decrease in dimensionless acoustic power, caused by slightly changed vortex dynamics. The perturbation amplitude has a considerably stronger effect (see Fig. 19b). The relation between $\langle P_s \rangle$ and $|u'_{ac}|/U_b$ is not linear, as in the intermediate amplitude regime (Section 3). Further study of the vortices occurring at high and low perturbation amplitude reveals that the differences are caused by the effect of the perturbation amplitude on the vortex dynamics. Vortices become less strong and are more diffuse when the acoustic velocity is lowered (compare Fig. 20a and b). This effect has also been visualized by for example Peters [55]. The local vorticity in the vortex core is also a function of $|u'_{ac}|$. The spatial distribution of the time-averaged source power, depicted in Fig. 18, reveals a postponed vortex formation, resulting in a reduction of the vorticity inside the vortices. Whereas for $|u'_{ac}|/U_b = 0.1$ the vortices appear at the end of the rounded upstream edge, for $|u'_{ac}|/U_b = 0.025$ this is postponed to almost halfway the cavity. The regions of absorption and production that co-exist at the upstream cavity edge in Fig. 18b show that vortex formation is not initiated yet at that position. The spatial extent of the production and absorption regions in the downstream half of the cavity is also smaller for lower disturbance amplitudes. Not all of the vorticity in the shear layer is, therefore, concentrated in discrete vortices, which is a requirement for the linear scaling to hold. At the present conditions the scaling is somewhere between the linear and the quadratic regime.

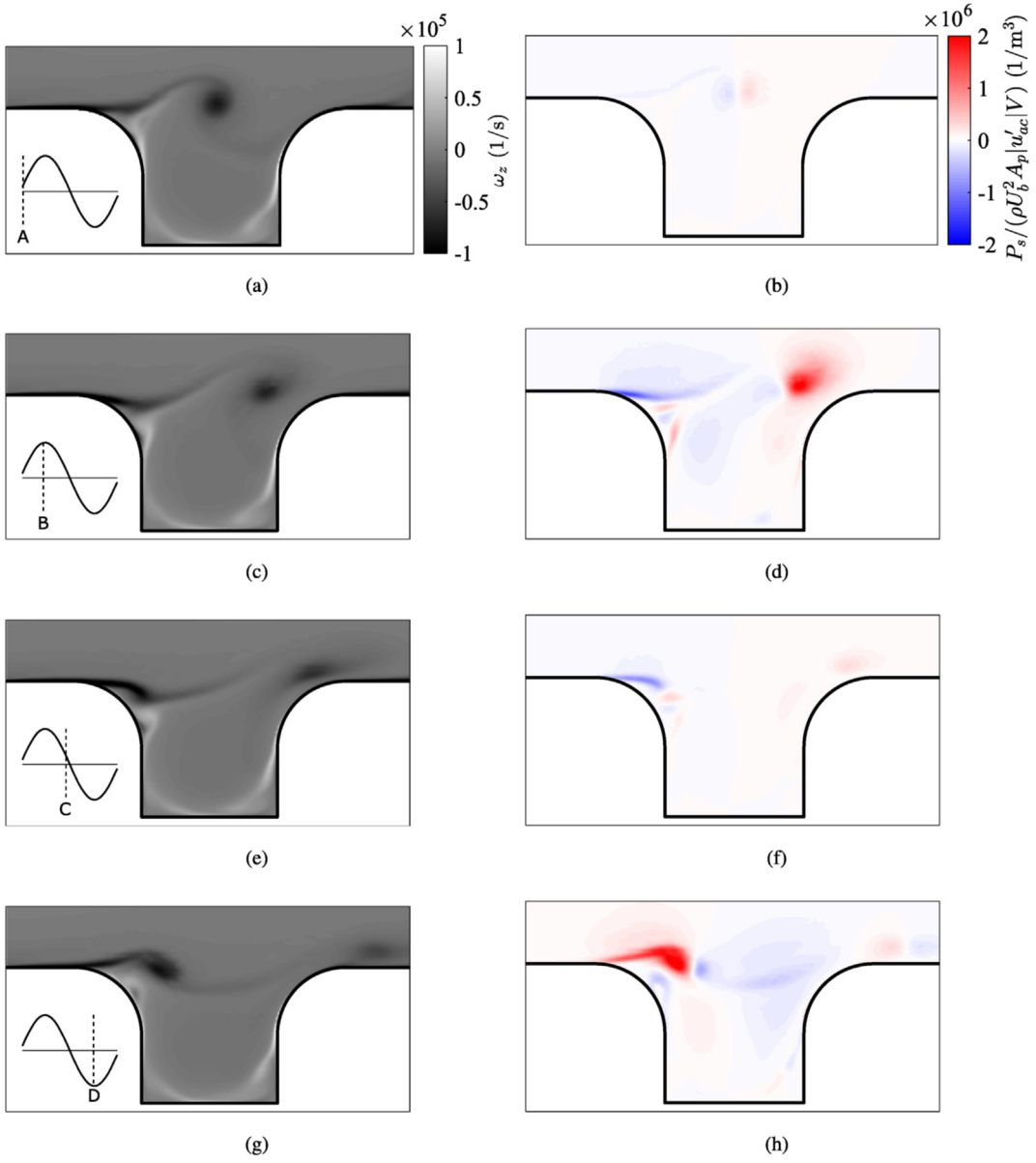

Fig. 17. Instantaneous vorticity contours (a, c, e, g) and source power contours (b, d, f, h) for the four instances tagged in Fig. 16b (geometry A). The position in the acoustic perturbation period is depicted in the bottom left of the vorticity contour plots.

7.3.3. Comparison to experiments

The numerical results can be compared to the measurements reported in Section 5. For that purpose, simulations are carried out at the perturbation amplitude observed in experiments. The peak-whistling Strouhal number for geometry A equals 0.36, both for the experiments and simulations. The dimensionless acoustic source power is, however, significantly higher than expected from the measurements reported in Table 2 (1.47×10^{-3} versus 0.8×10^{-3}). Previous studies found a similar discrepancy between experimental and numerical values for the source power [12]. Furthermore, in the derivation of the acoustic source strength, it is assumed that the source strength scales linearly with the perturbation amplitude to arrive at Eq. (6). It is shown previously that this scaling is not accurate. Assuming that $P_s = f(|u'_{ac}|^{1.5})$, the resulting source strength would be approximately 13% lower, bringing the experimental and numerical results closer together. Nonetheless, a difference remains, which is caused by both the simplifications in the model, and the assumptions made in the calculation of the acoustic losses in the experimental setup. Important to note is that the scaling to a power 1.5 of the source power with the acoustic amplitude complicates the comparison of experimental and numerical results using the EBM presented in Section 3.1. A slight change in source power or acoustic losses results in a large difference in whistling amplitude. The focus will therefore be on a comparison of the trends obtained from experiments and numerical simulations.

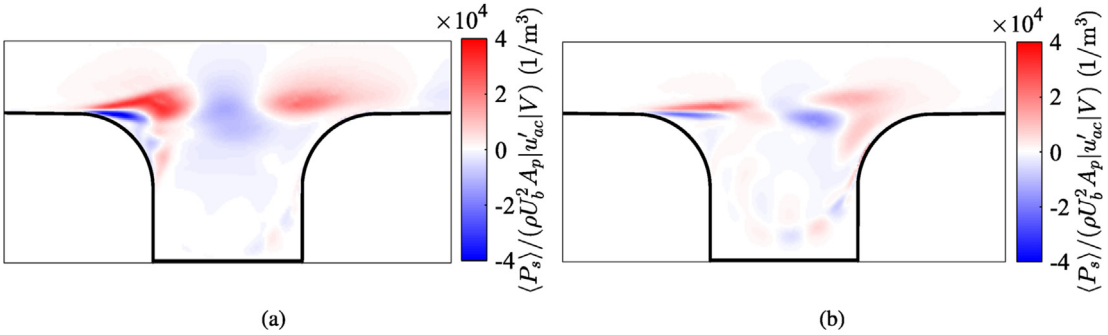

Fig. 18. Spatial distribution of time-averaged source power for geometry A, at the peak-whistling Strouhal number. The amplitude of the perturbation velocity is $|u'_{ac}|/U_b = 0.1$ (a) and 0.025 (b), for a bulk velocity of 40 m/s.

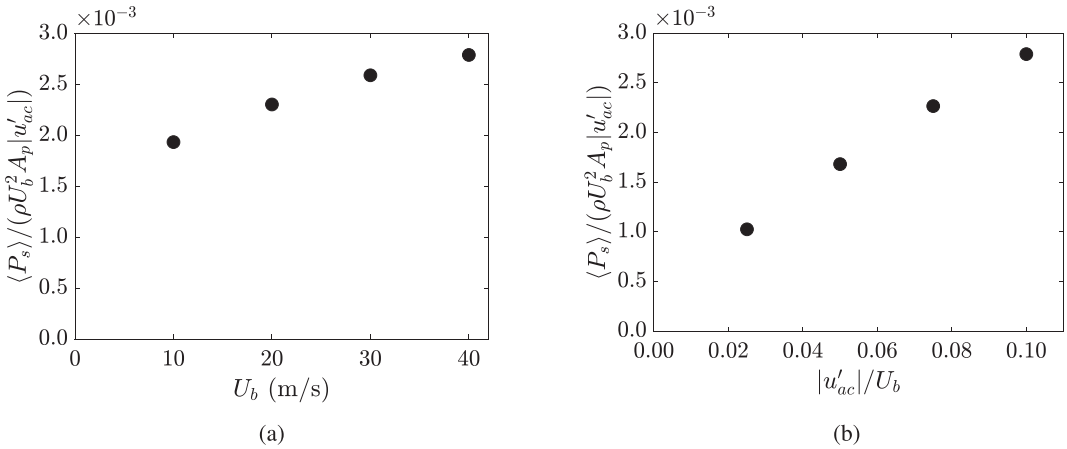

Fig. 19. Dimensionless acoustic source power as a function of the gas flow velocity (a) and the perturbation amplitude (b).

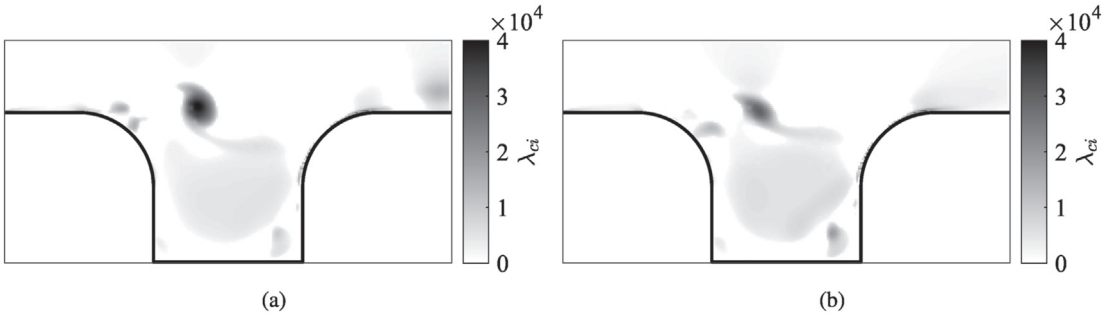

Fig. 20. Vortices traveling over the cavity mouth, visualized using the swirling strength criterion [54]. The amplitude of the perturbation velocity is $|u'_{ac}|/U_b = 0.1$ (a) and 0.025 (b), for a bulk velocity of 40 m/s.

Table 3
Comparison of the peak whistling Strouhal numbers for the geometries depicted in Fig. 3.

Geom	A	B	C	D	E
Sr_{pw} experimental [−]	0.36	0.30	0.28	0.41	0.35
Sr_{pw} numerical [−]	0.36	0.33	0.30	0.42	0.32
% change	0%	+10%	+7%	+2%	−8%

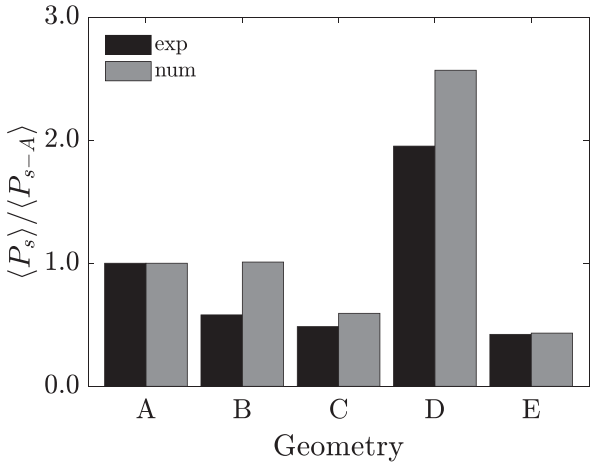

Fig. 21. Normalized acoustic source power obtained from URANS simulations and experiments, for the different geometries listed in Fig. 3 and Table 1.

7.4. Cavity geometry

Simulations are carried out for all geometries depicted in Fig. 3 with a fixed flow velocity and for a range of whistling frequencies. The perturbation amplitudes are taken form the experiments. The peak whistling Strouhal number for the different geometries shows good agreement with the experimental values (Table 3). The largest difference occurs for geometry B and amounts 10%, while the other geometries show results closer to the experimental value.

The source power is overestimated for all geometries by the simulations, as was also found for geometry A. The absolute values of the source power are a factor 1.5–2 higher in the simulations except for geometry B where the numerical results amount three times the experimental value. It should be noted that in the experiments, for the fixed flow velocity, the whistling does not always occur at the peak-whistling point. This could lead to a slight underestimation of the experimentally obtained whistling amplitude. However, this effect is small and does not explain the differences between experiments and simulations.[1] Normalizing the source power using the result for geometry A shows that the trends obtained from experiments and simulations are rather similar. Using this normalization (results are depicted in Fig. 21) accounts in part for inaccuracies in the estimation of the EBM terms. Only for the shallow geometry B the numerical trend deviates from the experiments. The numerical source power for this geometry matches that of the reference geometry, whereas in the experiments it whistled at significantly lower amplitudes. Nakiboğlu et al. [12] also observed a stronger deviation from experiments for shallower cavities in his simulations.

In Section 6 it is shown that this upstream edge is strongly altered by the presence of liquid. To assess the consequences of changed edge radii, simulations are carried out with the geometries depicted in Fig. 22. Geometries A_{2-4} are inspired by the reference geometry A, but have a sharp upstream or downstream edge. Simulations are carried out at a flow velocity of 40 m/s and a perturbation amplitude of 10%. The numerically obtained acoustic source power at peak-whistling frequency for these geometries is listed in Table 4. By sharpening the upstream edge (A_2) the acoustic source power is greatly reduced. When this geometry is inverted (A_4), now with the sharp edge at the downstream side, the source power is similar to that of geometry A and even slightly increased. A sharper edge results in a locally stronger directional change of the acoustic velocity. If this occurs at the upstream edge, the acoustic absorption region is intensified (compare Fig. 18a). The opposite happens if the downstream edge is sharp; the acoustic production increases in strength. This latter effect is less strong due to viscous spreading of the vortices. Sharpening the upstream edge also results in an effectively shortened cavity, as the shear layer separation point in geometry A is located just after the onset of the curvature. Geometry A_3 is therefore also modeled, where the cavity length is taken as $L_c + r_{edge}$. Still a 50% reduction of acoustic source power is obtained, substantiating the importance of the upstream edge radius.

[1] It is verified that a deviation of 5% of the perturbation frequency from the peak-whistling frequency, which is the maximum that could occur within a single plateau, does only account for a maximum variation in source power in the order of 5–10%.

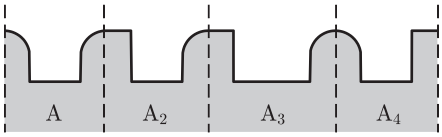

Fig. 22. Geometries based on geometry A, used to assess the effect of edge rounding on acoustic the source power.

Table 4
Peak whistling acoustic source power obtained for the geometries depicted in Fig. 22.

Geometry	A	A_2	A_3	A_4
$\langle P_s \rangle / (\rho U^2 A_p \lvert u'_{ac} \rvert)(\times 10^{-3})$	2.79	0.03	1.30	3.06

7.5. Liquid cavity filling - numerical

From the PLIF experiments described in Section 4.3 the profile of the liquid filling inside the cavities is obtained. These filling profiles for geometry A are used as an input for the numerical simulations to evaluate the effect of filling on the acoustic source strength. The gas-liquid interface is modeled as a solid wall, which is justified by the large difference in typical time scales for the gas and the liquid phase. The experimental filling profile is averaged in time and space and is assumed to be axisymmetric. For a gas flow velocity of 40 m/s, the filling profile at three different liquid flow rates is used. Fig. 23a shows the source power obtained from experiments, for different liquid volume fractions φ_l. The *energy balance model* is used to obtain those values (see Section 3.1). Point C1 in this figure is the dry reference case, and points C2, C3 and C4 are the liquid filling cases that are studied numerically. It should be noted that for case C4 no whistling is observed in the experiments.

The source strength from the URANS simulations with the filled cavities for cases C1–C4 is evaluated at the respective experimental whistling amplitude. Since the numerical source strength is always significantly higher compared to the experimental values, trends are compared here. Fig. 23b shows the normalized source power from experiments and numerical simulations for different liquid volume fractions. A good agreement is found between the experimentally and numerically obtained trends in Fig. 23h. In both the experiments and the simulations the source strength is reduced to around 25% of its reference value for a liquid volume fraction of 3.6×10^{-5}. Important to note is that the filling profile on top of the ribs separating the cavities is not measured; this profile is extrapolated from the filling inside the cavities. An example of this extrapolation is shown in Fig. 24. Nonetheless, a good agreement of the declining normalized source power is obtained in Fig. 23b.

8. Discussion

Several mechanisms are proposed in literature that could cause whistling mitigation in corrugated pipes by means of liquid addition. The most important mechanisms are (1) liquid cavity filling, (2) acoustic damping due to the presence of droplets and (3) shear layer disruption by liquid fragments. In previous work, focusing on a single corrugation geometry, it was proposed that liquid cavity filling is the major mechanism for whistling mitigation [24]. The liquid filling fraction (α) was used as the critical

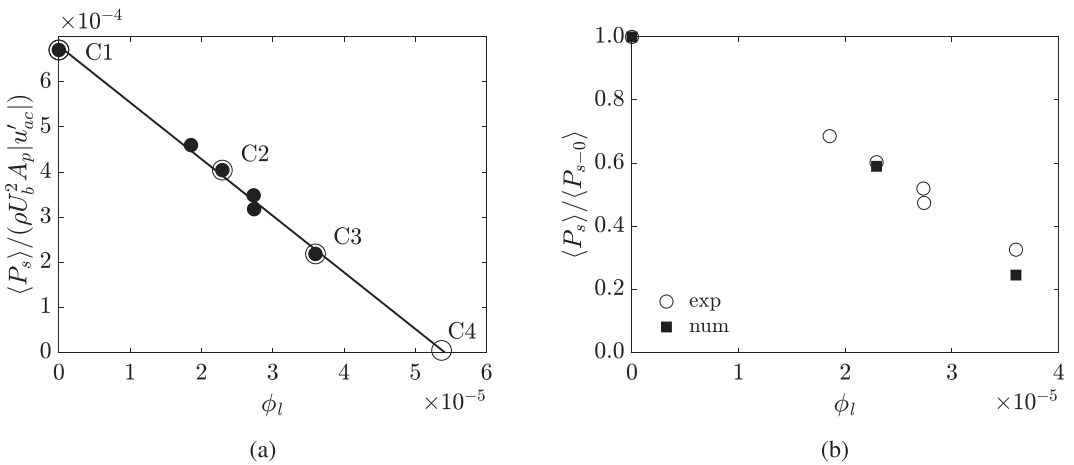

Fig. 23. (a) Acoustic source strength obtained from experiments with corrugation geometry A, versus the liquid volume fraction φ_l. The bulk gas flow velocity U_b is 40 m/s. Experimentally obtained filling profiles for four values of the liquid volume fraction are used to numerically obtain the source strength (C1-4). (b) Comparison of the normalized source power obtained from experiments and single phase simulations, as a function of liquid volume fraction for geometry A at a gas flow velocity of 40 m/s.

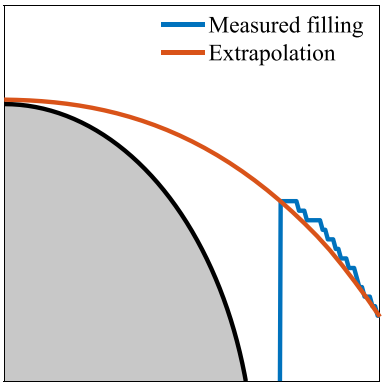

Fig. 24. Example of the extrapolation used at the upstream cavity edge for case C3 in Fig. 23a.

parameter, identifying to what extent the acoustic amplitude would be reduced. Droplet sizing measurement confirm that the acoustic damping due to the dispersed liquid phase is marginal, despite the very large liquid entrainment ratio in corrugated pipes compared to smooth pipes [40]. Furthermore, a corrugated pipe with a geometry similar to a liquid-filled cavity did not exhibit whistling in single phase conditions. Also the numerical results for geometry A with different liquid filling profiles support this. A similar reduction in source power is obtained from single-phase simulations, where only the cavity geometry is copied from the experiments. The presence of liquid in other regions of the pipe is not critical, as the main reduction is caused by the changed cavity geometry. Experiments with different cavity geometries (A and D) and different injected liquids (water and mono-ethylene glycol) show that the liquid filling fraction in itself is not sufficient to fully explain the reduction in whistling amplitude. Especially for water addition to geometry D and MEG addition to geometry A (Figs. 11 and 10b, respectively) a considerable spread of the critical value for α at which whistling disappears is observed. In general it holds that at higher gas flow speeds a smaller liquid filling of the cavities is sufficient to mitigate whistling. For geometry D (Figs. 11 and 12c) the spread in α at which whistling disappears is considerable: from $\alpha = 0.55$ at $U_b = 25$ m/s to $\alpha = 0.35$ at $U_b = 35$ m/s. For higher gas flow rates even lower critical filling fractions are expected. Fig. 12c shows the liquid filling profiles at the point of total whistling mitigation. The main difference is observed in the deeper part of the cavity, where the filling occurs in streamwise direction. In the cavity mouth, which is the actual source region, the profiles are very similar. The behavior of liquid in this region seems to be essential for the sound source amplitude. The deeper cavity part does not contribute significantly to the whistling. The filling fraction α, however, does reflect alterations of this deeper cavity part as well and is therefore not representative for the whistling mitigation. For geometry A, these observations also hold, but are less apparent. At full whistling mitigation the filling inside the cavity mouth decreases in extent when the gas flow rate increases. This is caused by the decreasing dimensionless whistling amplitude for increasing flow velocity in dry conditions (see Fig. 5b). At higher gas flow velocities, the point of whistling mitigation is therefore reached more easily. For geometry D this decrease in whistling amplitude at higher frequencies is less apparent, since the acoustic losses at the pipe ends are relatively smaller due to an increased source strength and a lower whistling frequency. For all cases it holds that a liquid filling of 60% of the cavity volume is sufficient to mitigate whistling entirely.

The numerical results underline these findings. The biggest contribution to sound production and absorption occurs in the cavity mouth. The deeper part of the cavity does not contribute significantly to the source power. Apart from the gas flow velocity and the perturbation amplitude, it is mainly determined by the shape of the upstream cavity edge and the spatial extent of the cavity mouth.

The results for the whistling behavior as a function of the cavity geometry can be combined with previous work on the two-phase flow behavior in corrugated pipes [40]. In that study, a relation between global flow parameters and local filling behavior is obtained for the cavity geometries also used in this study (geometry A and D). In the present work it is shown that the shape of the liquid surface for a certain filling ratio is crucial for the acoustic output of a certain geometry. This shape is determined by the dynamic balance between surface tension, gravity and inertial forces exerted by the gaseous internal cavity flow. Further study of the dependency of the filling (profile) on global flow parameters and geometry is required to use the model by Ref. [40] for predictive purposes.

9. Conclusions

Experiments and simulations are carried out to assess the effect of liquid addition to vertical upward corrugated pipe flow. In particular, the mechanisms behind whistling mitigation by liquid addition is studied. The whistling amplitude reduces linearly with increasing liquid volume fraction φ_l injected into the corrugated pipe. The liquid volume fraction required to mitigate whistling entirely increases with increasing gas flow rate. The effect of the liquid viscosity is very limited, the interfacial tension is more important. It is shown that additional acoustic damping due to the presence of a dispersed liquid phase in the bulk flow of the pipe does not contribute significantly to the reduction of whistling amplitude reduction. Cavity filling is the crucial

mechanism determining whistling mitigation in corrugated pipes. The whistling reduction is related to liquid present in the cavity mouth and the associated alteration of the cavity edge geometry. The presence of liquid is not a prerequisite to mitigate sound production. The geometrical change of the corrugations through the presence of liquid is, as is shown in single phase experiments. There are two main parameters that determine the source strength of a cavity geometry filled with liquid: the curvature of the upstream cavity edge, and the length of the cavity mouth. Furthermore, it is shown that the liquid volume fraction required for whistling to disappear is reduced by a factor three when the filling is not continuous in azimuthal direction. This occurs in the present experiments when the wall is strongly water repellent.

A numerical method is developed to gain more insight in the whistling cycle for different geometries. It consists of a 2D-axisymmetric incompressible URANS simulation, where vortex shedding is triggered by a velocity perturbation at the upstream boundary condition of the numerical domain. A separate numerically obtained potential flow solution for the same cavity geometry is used to calculate the acoustic velocity field. The results of both simulations are used in Howe's energy corollary to obtain an estimated sound source power. The advantage of the present method is that it provides more insight in the whistling cycle, and the spatial and temporal evolution of regions of acoustic production and absorption. Results obtained with this method for a reference case reported in literature closely match to previous studies using a different implementation of the same approach [12,51]. Assessing the different geometries numerically results in similar trends compared to the experiments. Only the results for the shallow cavity geometry deviate from the trend. It is reported in literature that comparable numerical methods have difficulties at low depth-over-length ratio cavities, and should not be applied for such geometries. In absolute terms, the source power is over-predicted by approximately a factor two in all cases. This is an acceptable over-prediction, given the simplicity of the numerical method. Furthermore, the comparison to experimental data is made using a partly theoretical energy balance method (EBM), which introduces uncertainties in the experimentally obtained source power. In the derivation of the EBM a linear dependency of the source power on the perturbation amplitude is assumed, but the simulations show that in the present regime the source power scales with $|u'_{ac}|^{1.5}$. The whistling Strouhal number is predicted to within 10% from the experimental values for all geometries. A negative correlation is found between the filling fraction and the acoustic source power in the simulations. The negative trend closely resembles experimentally obtained trends, underlining the conclusion that filling of the cavities with liquid is the principal mechanism determining whistling amplitude reduction in corrugated pipes with liquid addition.

CRediT authorship contribution statement

A.C. van Eckeveld: Conceptualization, Methodology, Software, Validation, Investigation, Writing - original draft. **J. Westerweel:** Supervision, Writing - review & editing. **C. Poelma:** Supervision, Writing - review & editing.

Declaration of competing interest

The authors declare that they have no known competing financial interests or personal relationships that could have appeared to influence the work reported in this paper.

Acknowledgements

This work is funded by Shell, for which they are gratefully acknowledged. The authors also thank E.F.J. Overmars, J. Ruijgrok and J. Graafland for their practical help in the design of the measurements and the experimental setup. A. Hirschberg is thanked for the valuable contribution that he had in various discussions on the topic.

References

[1] D. Rockwell, E. Naudascher, Self-sustaining oscillations of flow past cavities, J. Fluid Eng. 100 (1978) 152–165, https://doi.org/10.1115/1.3448624.
[2] X. Gloerfelt, Cavity noise, in: von Karman Lect. Notes Aerodyn. Noise from Wall-Bounded Flows, 2009.
[3] A. Michalke, On spatially growing disturbances in an inviscid shear layer, J. Fluid Mech. 23 (1965) 521–544, https://doi.org/10.1017/s0022112065001520.
[4] M.S. Howe, Theory of Vortex Sound, Cambridge University Press, 2003.
[5] A.M. Binnie, Self-induced waves in a conduit with corrugated walls ii. experiments with air in corrugated and finned tubes, in: Proceedings of the Royal Society of London A: Mathematical, Physical and Engineering Sciences, vol. 262, The Royal Society, 1961, pp. 179–191, https://doi.org/10.1098/rspa.1961.0111.
[6] J.W. Elliott, Corrugated pipe flow, in: M.C.M. Wright (Ed.), Lecture Notes on the Mathematics of Acoustics, Imperial College Press, 2005, pp. 207–222, https://doi.org/10.1142/9781860946554_0011.
[7] S.W. Rienstra, Fundamentals of Duct Acoustics, Eindhoven University of Technology, 2015.
[8] J. Bruggeman, A. Hirschberg, M. Van Dongen, A. Wijnands, J. Gorter, Self-sustained aero-acoustic pulsations in gas transport systems: experimental study of the influence of closed side branches, J. Sound Vib. 150 (1991) 371–393, https://doi.org/10.1016/0022-460x(91)90893-o.
[9] P. Martnez-Lera, C. Schram, S. Fller, R. Kaess, W. Polifke, Identification of the aeroacoustic response of a low mach number flow through a t-joint, J. Acoust. Soc. Am. 126 (2009) 582–586, https://doi.org/10.1121/1.3159604.
[10] G. Nakibolu, S.P.C. Belfroid, J.F.H. Willems, A. Hirschberg, Whistling behavior of periodic systems: corrugated pipes and multiple side branch system, Int. J. Mech. Sci. 52 (2010) 1458–1470, https://doi.org/10.1016/j.ijmecsci.2010.03.018.
[11] O. Rudenko, G. Nakibolu, A. Holten, A. Hirschberg, On whistling of pipes with a corrugated segment: experiment and theory, J. Sound Vib. 332 (2013) 7226–7242, https://doi.org/10.1016/j.jsv.2013.08.034.
[12] G. Nakibolu, H. Manders, A. Hirschberg, Aeroacoustic power generated by a compact axisymmetric cavity: prediction of self-sustained oscillation and influence of the depth, J. Fluid Mech. 703 (2012a) 163–191, https://doi.org/10.1017/jfm.2012.203.
[13] M. Gharib, A. Roshko, The effect of flow oscillations on cavity drag, J. Fluid Mech. 177 (1987) 501–530, https://doi.org/10.1017/s002211208700106x.

[14] G. Nakibolu, S. Belfroid, J. Golliard, A. Hirschberg, On the whistling of corrugated pipes: effect of pipe length and flow profile, J. Fluid Mech. 672 (2011) 78–108, https://doi.org/10.1017/s0022112010005884.
[15] S. Dequand, S.J. Hulshoff, A. Hirschberg, Self-sustained oscillations in a closed side branch system, J. Sound Vib. 265 (2003) 359–386, https://doi.org/10.1016/s0022-460x(02)01458-x.
[16] M. Bolduc, M. Elsayed, S. Ziada, Effect of upstream edge geometry on the trapped mode resonance of ducted cavities, in: ASME 2013 Pressure Vessels and Piping Conference, American Society of Mechanical Engineers, 2013, https://doi.org/10.1115/pvp2013-97149. V004T04A028V004T04A028.
[17] D. Tonon, B.J.T. Landry, S.P.C. Belfroid, J.F.H. Willems, G.C.J. Hofmans, A. Hirschberg, Whistling of a pipe system with multiple side branches: comparison with corrugated pipes, J. Sound Vib. 329 (2010) 1007–1024, https://doi.org/10.1016/j.jsv.2009.10.020.
[18] A. Kierkegaard, S. Allam, G. Efraimsson, M. bom, Simulations of whistling and the whistling potentiality of an in-duct orifice with linear aeroacoustics, J. Sound Vib. 331 (2012) 1084–1096.
[19] B. Rajavel, M. Prasad, Acoustics of corrugated pipes: a review, Appl. Mech. Rev. 65 (2013), https://doi.org/10.1115/1.4025302.
[20] A. Petrie, I. Huntley, The acoustic output produced by a steady airflow through a corrugated duct, J. Sound Vib. 70 (1980) 1–9, https://doi.org/10.1016/0022-460x(80)90551-9.
[21] M. Gharib, Active Control of Flow Induced Resonance in Continuous Corrugated Tubes, DTIC Document, 1993. Technical Report.
[22] S. Belfroid, J. Golliard, O. Vijlbrief, Singing mitigation in corrugated tubes with liquid injection, in: ASME 2013 Pressure Vessels and Piping Conference, American Society of Mechanical Engineers, 2013, https://doi.org/10.1115/pvp2013-97973.
[23] J. Golliard, S. Belfroid, O. Vijlbrief, Acoustic damping in smooth and corrugated pipes with and without liquid injection, in: ASME 2013 Pressure Vessels and Piping Conference, American Society of Mechanical Engineers, 2013, https://doi.org/10.1115/pvp2013-97970.
[24] A.C. van Eckeveld, J. Westerweel, C. Poelma, Mitigation of whistling in vertical corrugated pipes by liquid addition, Exp. Fluid 58 (2017) 107, https://doi.org/10.1007/s00348-017-2391-1.
[25] J.C. Bruggeman, A.P.J. Wijnands, J. Gorter, Self sustained low frequency resonance in low-mach-number gas flow through pipe-lines with side-branch cavities: a semi-empirical model, in: 10th Aeroacoustics Conference, 1986, pp. 86–1924, https://doi.org/10.2514/6.1986-1924.
[26] M. Howe, The dissipation of sound at an edge, J. Sound Vib. 70 (1980) 407–411.
[27] C. Weng, Theoretical and Numerical Studies of Sound Propagation in Low-Mach-Number Duct Flows, KTH Royal Institute of Technology, 2015. Ph.D. thesis.
[28] E. Dokumaci, Sound transmission in narrow pipes with superimposed uniform mean flow and acoustic modelling of automobile catalytic converters, J. Sound Vib. 182 (1995) 799–808, https://doi.org/10.1006/jsvi.1995.0233.
[29] D. Ronneberger, C. Ahrens, Wall shear stress caused by small amplitude perturbations of turbulent boundary-layer flow: an experimental investigation, J. Fluid Mech. 83 (1977) 433–464, https://doi.org/10.1017/s0022112077001281.
[30] S. Belfroid, N. Gonzlez Dez, J. Golliard, K. Lunde, S. Naess, Damping and source strength characteristics of corrugated pipes: influence gap width, in: Proceedings of the 9th International Symposium on Fluid-Structure Interactions, Flow-Sound Interactions, Flow-Induced Vibration & Noise, 2018.
[31] H. Levine, J. Schwinger, On the radiation of sound from an unflanged circular pipe, Phys. Rev. 73 (1948) 383–406, https://doi.org/10.1103/physrev.73.383.
[32] A.N. Norris, I.C. Sheng, Acoustic radiation from a circular pipe with an infinite flange, J. Sound Vib. 135 (1989) 85–93, https://doi.org/10.1016/0022-460x(89)90756-6.
[33] A. Hirschberg, S.W. Rienstra, An Introduction to Aeroacoustics, Eindhoven University of Technology, 2004.
[34] S.-H. Jang, J.-G. Ih, On the multiple microphone method for measuring in-duct acoustic properties in the presence of mean flow, J. Acoust. Soc. Am. 103 (1998) 1520–1526, https://doi.org/10.1121/1.421289.
[35] U. Ingard, V.K. Singhal, Effect of flow on the acoustic resonances of an open-ended duct, J. Acoust. Soc. Am. 58 (1975) 788–793, https://doi.org/10.1121/1.380751.
[36] P.O.A.L. Davies, Plane wave reflection at flow intakes, J. Sound Vib. 115 (1987) 560–564, https://doi.org/10.1016/0022-460x(87)90298-7.
[37] R.M. Munt, The interaction of sound with a subsonic jet issuing from a semi-infinite cylindrical pipe, J. Fluid Mech. 83 (1977) 609–640, https://doi.org/10.1017/s0022112077001384.
[38] R.M. Munt, Acoustic transmission properties of a jet pipe with subsonic jet flow: I. the cold jet reflection coefficient, J. Sound Vib. 142 (1990) 413–436, https://doi.org/10.1016/0022-460x(90)90659-n.
[39] M.C.A.M. Peters, A. Hirschberg, A.J. Reijnen, A.P.J. Wijnands, Damping and reflection coefficient measurements for an open pipe at low mach and low helmholtz numbers, J. Fluid Mech. 256 (1993) 499–534, https://doi.org/10.1017/s0022112093002861.
[40] A.C. van Eckeveld, E. Gotfredsen, J. Westerweel, C. Poelma, Annular two-phase flow in vertical smooth and corrugated pipes, Int. J. Multiphas. Flow 109 (2018) 150–163, https://doi.org/10.1016/j.ijmultiphaseflow.2018.07.004.
[41] P.S. Epstein, R.R. Carhart, The absorption of sound in suspensions and emulsions. i. water fog in air, J. Acoust. Soc. Am. 25 (1953) 553–565, https://doi.org/10.1121/1.1907107.
[42] N. Curle, The influence of solid boundaries upon aerodynamic sound, in: Proceedings of the Royal Society of London A: Mathematical, Physical and Engineering Sciences, vol. 231, The Royal Society, 1955, pp. 505–514, https://doi.org/10.1098/rspa.1955.0191.
[43] M. Howe, Attenuation of sound in a low mach number nozzle flow, J. Fluid Mech. 91 (1979) 209–229.
[44] A. Powell, Theory of vortex sound, J. Acoust. Soc. Am. 36 (1964) 177–195, https://doi.org/10.1121/1.1918931.
[45] D.R. Lide, CRC Handbook of Chemistry and Physics, 75 ed., CRC press, 1994.
[46] D. Schubring, A.C. Ashwood, T.A. Shedd, E.T. Hurlburt, Planar laser-induced fluorescence (PLIF) measurements of liquid film thickness in annular flow. Part I: methods and data, Int. J. Multiphas. Flow 36 (2010) 815–824, https://doi.org/10.1016/j.ijmultiphaseflow.2010.02.002.
[47] A. Glover, S. Skippon, R. Boyle, Interferometric laser imaging for droplet sizing: a method for droplet-size measurement in sparse spray systems, Appl. Optic. 34 (1995) 8409–8421, https://doi.org/10.1364/ao.34.008409.
[48] K.J. Hay, Z.-C. Liu, T.J. Hanratty, Relation of deposition to drop size when the rate law is nonlinear, Int. J. Multiphas. Flow 22 (1996) 829–848, https://doi.org/10.1016/0301-9322(96)00029-8.
[49] V. Sarohia, Experimental and Analytical Investigation of Oscillations in Flows over Cavities, California Institute of Technology, 1975. Ph.D. thesis.
[50] H.H. Heller, D.B. Bliss, Flow-induced pressure fluctuations in cavities and concepts for their suppression, Aeroacoustics: STOL Noise, Airframe and Airfoil Noise 45 (1976) 281–296, https://doi.org/10.2514/5.9781600865190.0281.0296.
[51] J. Golliard, N. Gonzlez-Dez, S. Belfroid, G. Nakibolu, A. Hirschberg, U-rans model for the prediction of the acoustic sound power generated in a whistling corrugated pipe, in: ASME 2013 Pressure Vessels and Piping Conference, American Society of Mechanical Engineers, 2013, https://doi.org/10.1115/pvp2013-97385. V004T04A040V004T04A040.
[52] F.M. White, Fluid Mechanics, fourth ed., McGraw-hill, 2017.
[53] P. Nelson, N. Halliwell, P. Doak, Fluid dynamics of a flow excited resonance, part ii: flow acoustic interaction, J. Sound Vib. 91 (1983) 375–402, https://doi.org/10.1016/0022-460x(83)90287-0.
[54] J. Zhou, R.J. Adrian, S. Balachandar, T.M. Kendall, Mechanisms for generating coherent packets of hairpin vortices in channel flow, J. Fluid Mech. 387 (1999) 353–396, https://doi.org/10.1017/s002211209900467x.
[55] M.C.A.M. Peters, Aeroacoustic Sources in Internal Flows, Eindhoven University of Technology, 1993. Ph.D. thesis.